Contents lists available at ScienceDirect

International Journal of Machine Tools and Manufacture

journal homepage: www.elsevier.com/locate/ijmactool

Research Article

Atomic-scale smoothing of semiconducting oxides via plasma-enabled atomic-scale reconstruction

Yongjie Zhang [a,b], Jin Tang [a], Shaoxiang Liang [a], Junlei Zhao [c], Mengyuan Hua [c], Chun Zhang [b], Hui Deng [a,*]

[a] Department of Mechanical and Energy Engineering, Southern University of Science and Technology, Shenzhen, 518055, Guangdong, China
[b] Department of Physics and Centre for Advanced 2D Materials, National University of Singapore, 2 Science Drive 3, Singapore, 117551, Singapore
[c] Department of Electrical and Electronic Engineering, Southern University of Science and Technology, Shenzhen, 518055, Guangdong, China

ARTICLE INFO

Handling Editor: Dragos Axinte

Keywords:
Single crystal β-Ga_2O_3
Semiconducting oxides
Surface reconstruction
Atomic-scale smoothing
Atmospheric plasma
Atomic-scale manufacturing

ABSTRACT

β-Ga_2O_3, known as a next-generation wide-bandgap transparent semiconducting oxide (TSO), has considerable application potential in ultra-high-power and high-temperature devices. However, fabricating a smooth β-Ga_2O_3 substrate is challenging owing to its strong mechanical strength and chemical stability. In this study, an atomic-scale smoothing method named plasma-enabled atomic-scale reconstruction (PEAR) is proposed. We find that three reconstruction modes, namely, 2D-island, step-flow, and step-bunching, can be identified with the increase in the input power; only the step-flow mode can result in the formation of an atomically smooth β-Ga_2O_3 surface (Sa = 0.098 nm). Various surface and subsurface characterizations indicate that the smooth β-Ga_2O_3 surface shows excellent surface integrity, high crystalline quality, and remarkable photoelectric properties. The atomic-scale density functional theory-based calculations show that the diffusion energy barrier of a Ga atom is only 0.46 eV, thereby supporting the atomic mass migration induced by high-energy plasma irradiation in the experiment. Nanoscale molecular dynamics simulations reveal that O atoms firstly migrate to crystallization sites, followed by Ga atoms with a lower migration rate; reconstruction mainly proceeds along the <010> direction and then expands along the <100> and <001> directions. The millimeter-scale numerical simulations based on the finite element method demonstrate that the coupling of the thermal and flow fields of plasma is the impetus for PEAR of β-Ga_2O_3. Furthermore, the smoothing generality of PEAR is demonstrated by extending it to other common TSOs (α-Al_2O_3, ZnO, and MgO). As a typical plasma-based atomic-scale smoothing method, PEAR is expected to enrich the theoretical and technological knowledge on atomic-scale manufacturing.

1. Introduction

Gallium oxide (Ga_2O_3), as an emerging ultra-wide-bandgap transparent semiconducting oxide (TSO), has been garnering increasing research attention [1]. It is widely considered as the next-generation semiconducting material, surpassing conventional first-, second-, and third-generation semiconductors [1,2]. Six Ga_2O_3 types have been discovered and denoted as α-, β-, γ-, κ-, δ-, and ε-Ga_2O_3 [3]. Among these polytypes, β-Ga_2O_3 is the most stable and thus, has attracted most of the scientific and technological interest [1,3]. β-Ga_2O_3 exhibits remarkable electronic properties, compared with Si, GaAs, 4H–SiC, and GaN. For example, β-Ga_2O_3 possesses an ultra-wide bandgap of approximately 4.85 eV, and its breakdown field can be as high as 8 MV/cm [3]. Additionally, β-Ga_2O_3 has a high melting point of 1793 °C [3]. These properties make β-Ga_2O_3 a promising candidate for use in ultra-high-power and high-temperature application scenarios. These scenarios often require high-performance power semiconductor devices, including (but not limited to) metal-semiconductor field effect transistors [4], metal-oxide-semiconductor field effect transistors [5], Schottky barrier diodes [6], and solar-blind ultraviolet photodetectors [7], all of which are in substantial demand.

An atomic-scale smooth surface with a low density of defects is always necessary to maximize the performance of β-Ga_2O_3-based electronic devices. However, a few studies have been focused on the precision machining, especially the atomic-scale polishing, of β-Ga_2O_3, which is a representative difficult-to-machine material owing to its high mechanical strength and chemical stability [8]. Chemical mechanical polishing (CMP), which is the most widely used polishing method, has

* Corresponding author.
E-mail address: dengh@sustech.edu.cn (H. Deng).

https://doi.org/10.1016/j.ijmachtools.2024.104119
Received 2 November 2023; Received in revised form 28 December 2023; Accepted 6 January 2024

been preliminarily explored to smooth β-Ga_2O_3 [8,9]. As the name suggests, CMP involves slurry-based surface chemical modification, followed by abrasive-based mechanical removal of the modified layer. Studies have shown that the slurry, abrasive, and applied pressure are three key factors during the CMP of β-Ga_2O_3 [8,9]. Under acidic conductions, β-Ga_2O_3 is converted to Ga^{3+}-containing species; under alkaline conditions, $[Ga(OH_4)]^-$-containing species are identified [8, 10]. Specifically, in phosphoric acid slurry (pH = 3.8), the final root-mean-square roughness (*R*q) and material removal rate (MRR) were found to be 0.21 nm and 0.832 μm/h, respectively; in sodium

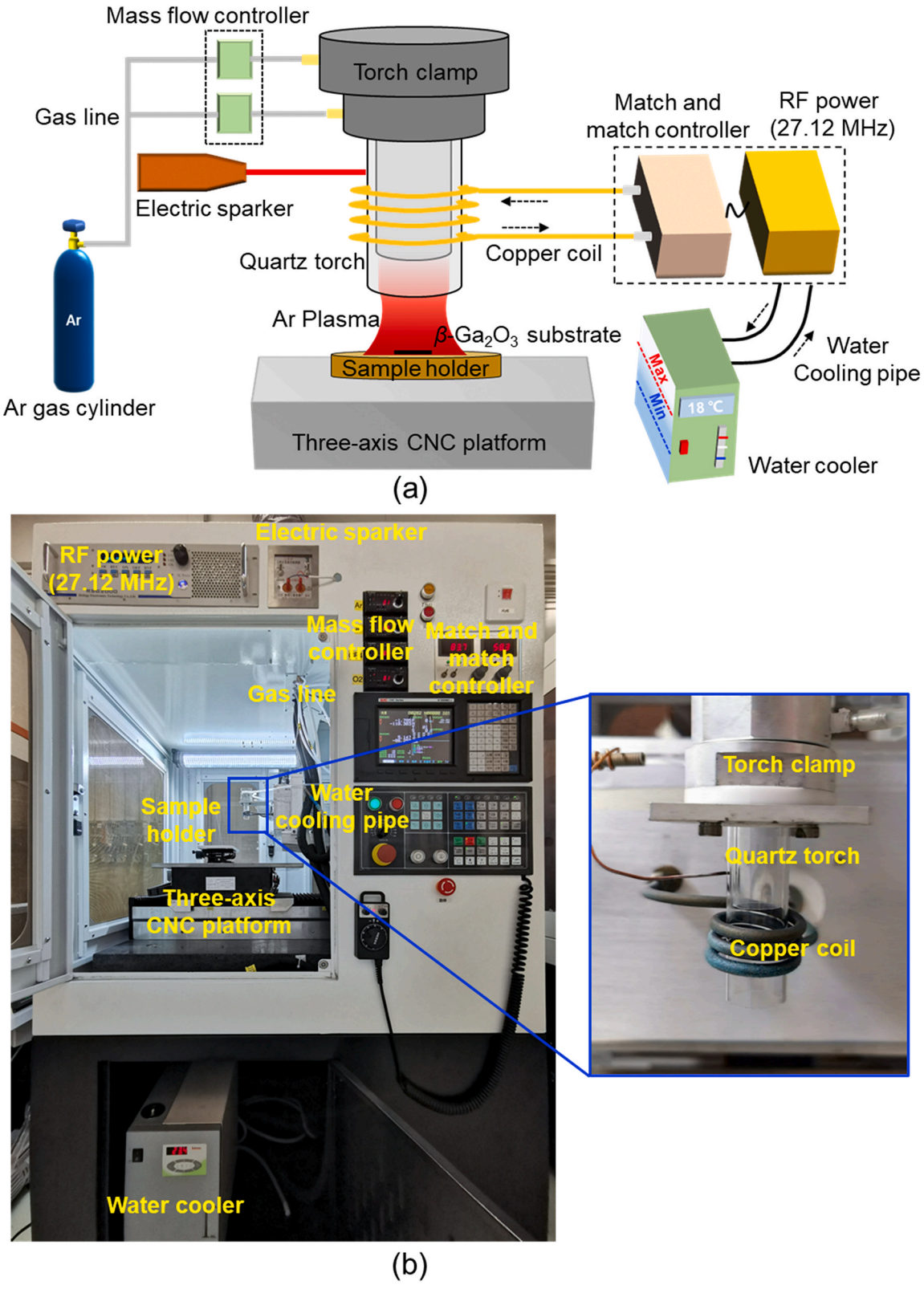

Fig. 1. Plasma setup. (a) Schematic diagram and (b) optical image of the setup. The inset in (b) shows the plasma generation part.

hydroxide slurry (pH = 10.6), the *R*q roughness was 0.48 nm and the MRR was 0.657 μm/h [8]. These results indicate that acidic conditions might be better than alkaline ones for the CMP of β-Ga_2O_3. In terms of the performance of abrasives, a MRR of ~1.3 μm/h was achieved when using colloidal alumina; this value is approximately three times larger than that achieved when using colloidal silica (~0.4 μm/h) [9]. However, colloidal silica was better for removing the subsurface damage. Additionally, high pressures (>10 kPa) are generally adopted in CMP to increase the MRR; however, such high pressures would inevitably cause subsurface damage [9,11]. Overall, three issues still remain in the fabrication of a smooth β-Ga_2O_3 surface via CMP. First, the processing efficiency is low, as the processing time is greater than 10 h and the MRR is smaller than 1 μm/h in general. Second, achieving an atomically perfect β-Ga_2O_3 surface via CMP is still challenging owing to the large size and random movement of abrasives. Third, completely removing the subsurface damage layer is difficult.

In addition to CMP, wet chemical etching (WCE) [12] and high temperature annealing (HTA) [13] have a certain ability to reduce the surface roughness of β-Ga_2O_3. In WCE, the removal of β-Ga_2O_3 is completely dependent on specific chemical reactions [14,15]. For example, Zhang et al. [14] proposed that root-mean-square roughness (RMS) of β-Ga_2O_3 could be decreased from 1.72 to 1.35 nm within 30 min by etching in phosphoric acid solution at 160 °C. In HTA, no material is removed; however, the material transfer caused by the high temperature leads to a change of surface roughness [16,17]. For example, Rafique et al. [16] declared that annealing in oxygen at 1000 °C for 1 h would result in RMS roughness reduction from 10.1 to 6.87 nm for β-Ga_2O_3. These studies demonstrate that WCE and HTA can only slightly reduce the surface roughness of β-Ga_2O_3 and that the final surfaces are generally not suitable for meeting the requirements of manufacturing high-performance electronic devices. The advantage of WCE is that different patterns can be fabricated on β-Ga_2O_3 via anisotropic etching [14], whereas HTA can improve surface crystalline quality [17]. No advanced polishing processes based on WCE or HTA have been proposed.

Achieving the atomic-scale, damage-free, and highly efficient smoothing of β-Ga_2O_3 by using the traditional mechanical, physical, and chemical processes is difficult. Thus, developing advanced polishing technologies for this promising semiconductor is critical. Atmospheric plasma, which has extremely strong physical and chemical properties, is a promising tool for ultraprecision polishing of difficult-to-machine materials. Fang et al. [18] proposed a plasma-based atom-selective etching (PASE) method that can achieve damage-free and atomic-scale polishing of single-crystal Si. In PASE, the adopted plasma is an atmospheric inductively coupled plasma (ICP), with Ar as the ignition and cooling gas, and CF_4 and O_2 as the reaction gases. Based on the etching effect of generated F radicals, Si atoms with more dangling bonds on the surface are preferentially removed with the formation of gaseous SiF_4, ultimately forming an ultrasmooth surface with all atoms in the same bonding state. It was demonstrated that a severely damaged Si (100) surface with the arithmetical mean height (*S*a) roughness of 195.67 nm was polished to the smooth state with the *S*a roughness of 0.71 nm. Obviously, PASE is a purely chemical removal process by etching radicals in plasma. Although an ultrasmooth surface could be obtained, its principle of forming an atomic-scale equipotential surface determines that it is difficult and even impossible to form the atomic step-terrace structure which is very important for subsequent semiconductor manufacturing processes such as epitaxial growth.

A further development of PASE is the hybrid utilization of the chemical and physical properties of plasma. By removing reaction gases from the atmospheric ICP, the chemical action of the ICP can be completely suppressed, allowing the ICP to operate in the physical mode. Deng et al. [19] claimed that the atomic-scale sapphire surfaces were farbricated via chemical-physical tuning of the ICP. With sliced rough sapphire as the original surface, the ICP in the chemical PASE mode (with CF_4 and O_2 as the reaction gases) was first adopted to etch the rough surface. Both the amorphous layer and the subsurface damage layer were removed during the etching process, eventually resulting in an ultrasmooth sapphire surface with the *S*a roughness of 0.067 nm. The ICP in physical mode (without reaction gases) was then used to induce surface reconstruction on the near-perfect crystalline surface, leading to the formation of an atomic step-terrace structure. Obviously, the formation of the step-terrace surface under the physical mode is on the basis that the amorphous layer and the subsurface damage layer were completely removed and an atomically smooth crystalline surface was obtained by the PASE process. Fabricating the step-terrace surface directly from a rough and damaged surface through the physical mode of plasma has not been realized yet.

For practical process flow of semiconductor wafers, wafer finishing usually starts with mechanically damaged surfaces processed by mechanical lapping or polishing. For a damaged surface with scratches, cracks, amorphous layer, and even subsurface damage, it is strongly desired to directly transform the damaged surface into a perfectly crystalline state with well-ordered atomic step-terrace structures. However, this is very challenging. Inspired by the aforementioned plasma-based studies [18,19], we propose a plasma-enabled atomic-scale reconstruction (PEAR) process, in which various TSOs with damaged surfaces can be transformed to atomically smooth surfaces with well-ordered step-terrace structures simply through the utilization of nonreactive plasma.

The core of PEAR is the atomic-scale reconstruction of a damaged surface after obtaining energy from plasma. Specifically, it is the recovery of the subsurface damage layer, the recrystallization of the amorphous layer, and the formation of atomic step-terrace structure on the surface under the coupling effect of thermal and flow fields of plasma. PEAR is conducted under atmospheric environment making it a promising approach for practical processing of large-size wafers. Finally, because the energy range of the plasma is precisely adjustable, the surface reconstruction of a variety of TSOs can be realized, making the PEAR process a universal approach for atomic surface manufacturing.

Focusing on the challenges for atomic surface manufacturing of β-Ga_2O_3 and other TSOs, we aim to develop the PEAR to efficiently transform a damaged surface into an atomically smooth surface with step-terrace structure. PEAR was proved to have the capability to decrease the surface roughness to the sub-angstrom level and improve the crystalline quality to a near-perfect level. The essence of PEAR is atomic-scale reconstruction induced by plasma under the physical mode, and the intrinsic impetus in surface reconstruction was experimentally and theoretically verified to be the coupled thermal and flow fields. Moreover, the migration energy barrier of a Ga atom, diffusion behaviors of Ga and O atoms, and priority of crystallization along different crystal orientations were theoretically investigated and discussed. This study provides valuable insights into the process and mechanism of plasma-enabled surface reconstruction of β-Ga_2O_3 and offers an alternative approach for atomic-scale manufacturing of TSOs.

2. Experimental methodology

2.1. Atmospheric pure Ar plasma

Pure Ar plasma generated at atmospheric pressure is adopted in this study, and a schematic diagram of the ICP setup is shown in Fig. 1a. This setup consists of five main parts: the plasma generation part (torch clamp and quartz torch), power supply part (radio frequency (RF) power, match and match controller, inductance coil, and electric sparker), gas supply part (Ar gas cylinder, mass flow controller, and gas line), water-cooling part (water cooler and pipe), and computer numerical control (CNC) machining system (three-axis platform and sample holder). Fig. 1b shows an optical image of the ICP setup, with an overview of the processing configuration and an enlarged view of the plasma generation part. High-purity Ar gas (≥99.999 %) is used to generate plasma without the addition of any reaction gas. Further details

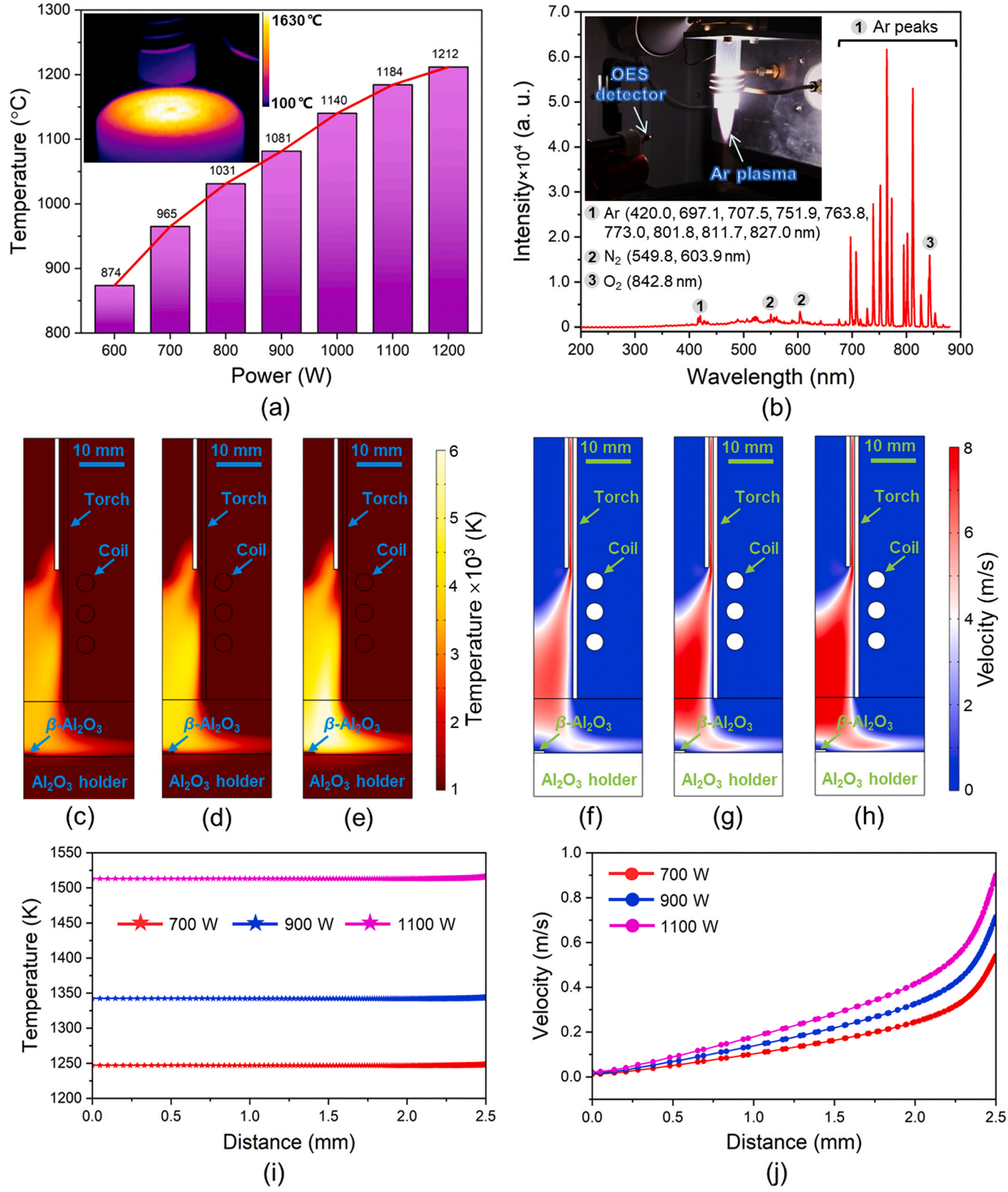

Fig. 2. Plasma diagnostics and numerical simulation results. (a) Variation of β-Ga_2O_3 (010) surface temperature with radio frequency (RF) power. The inset shows the temperature distribution at 900 W. (b) Optical emission spectroscopy (OES) results at 900 W. The inset shows the OES measurement setup. (c)–(e) Temperature simulation at 700, 900, and 1100 W, respectively. (f)–(h) Velocity simulation at 700, 900, and 1100 W, respectively. (i) Temperature and (j) velocity distributions from the sample surface's center to its edge.

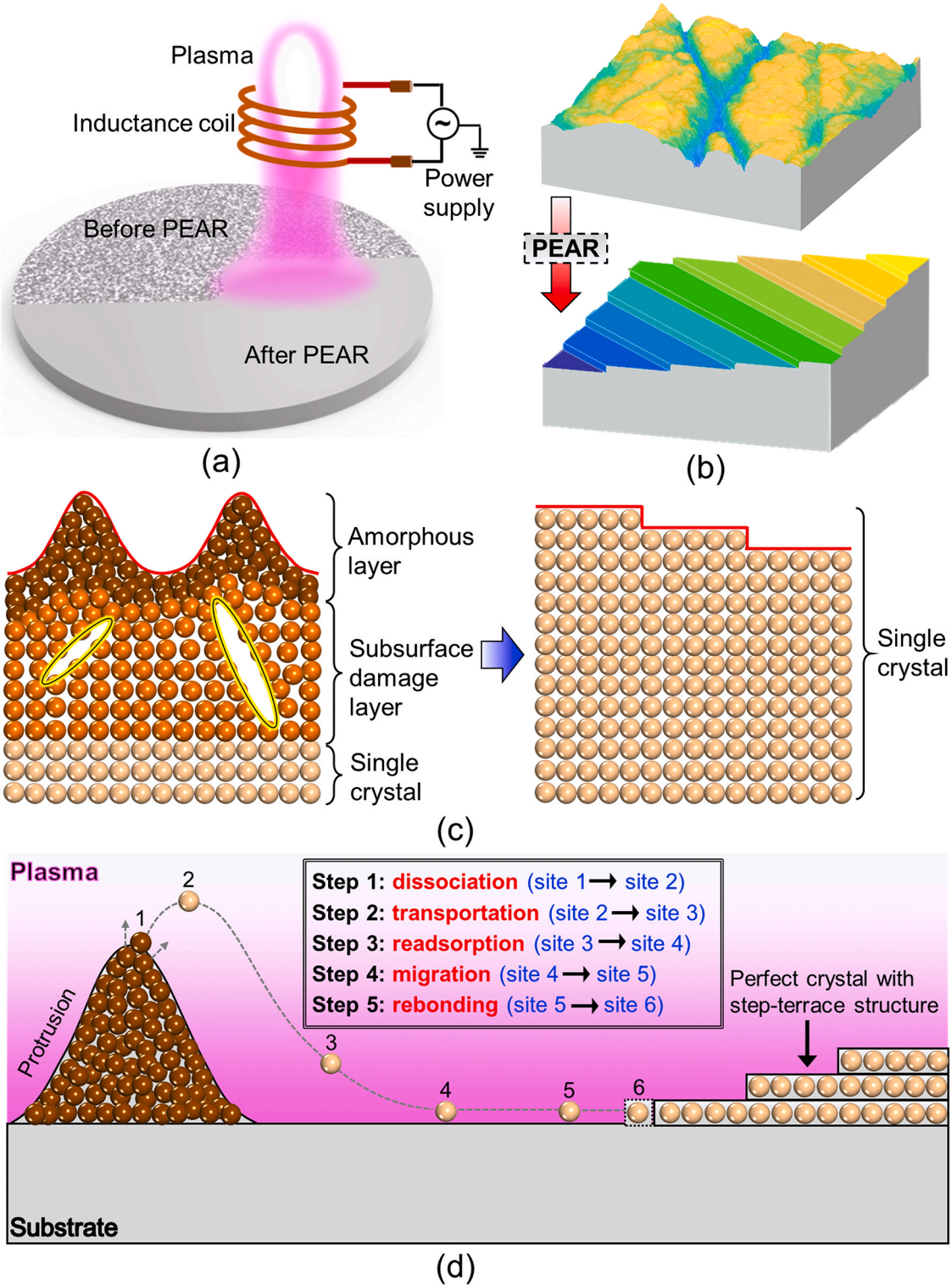

Fig. 3. Schematic diagram of plasma-enabled atomic-scale reconstruction (PEAR). (a) PEAR processing for a transparent semiconducting oxide (TSO) wafer. (b) Schematic surface morphologies before and after PEAR at the micron scale. (c) Schematic cross-sections before and after PEAR at the atomic scale. (d) Possible reconstruction process to form step-terrace structure.

on the plasma setup and excitation process can be found in Section 1 of the supplementary information, and the plasma static and scanning irradiation processes are shown in supplementary Video 1.

Supplementary video related to this article can be found at https://doi.org/10.1016/j.ijmachtools.2024.104119

2.2. Plasma diagnostics

First, we evaluated the substrate surface temperature at different RF powers using an infrared thermal imager. As shown in Fig. 2a, the surface temperature increases with an increasing RF power. At 600 W, the measured temperature is 874 °C; at 900 W, the temperature is close to

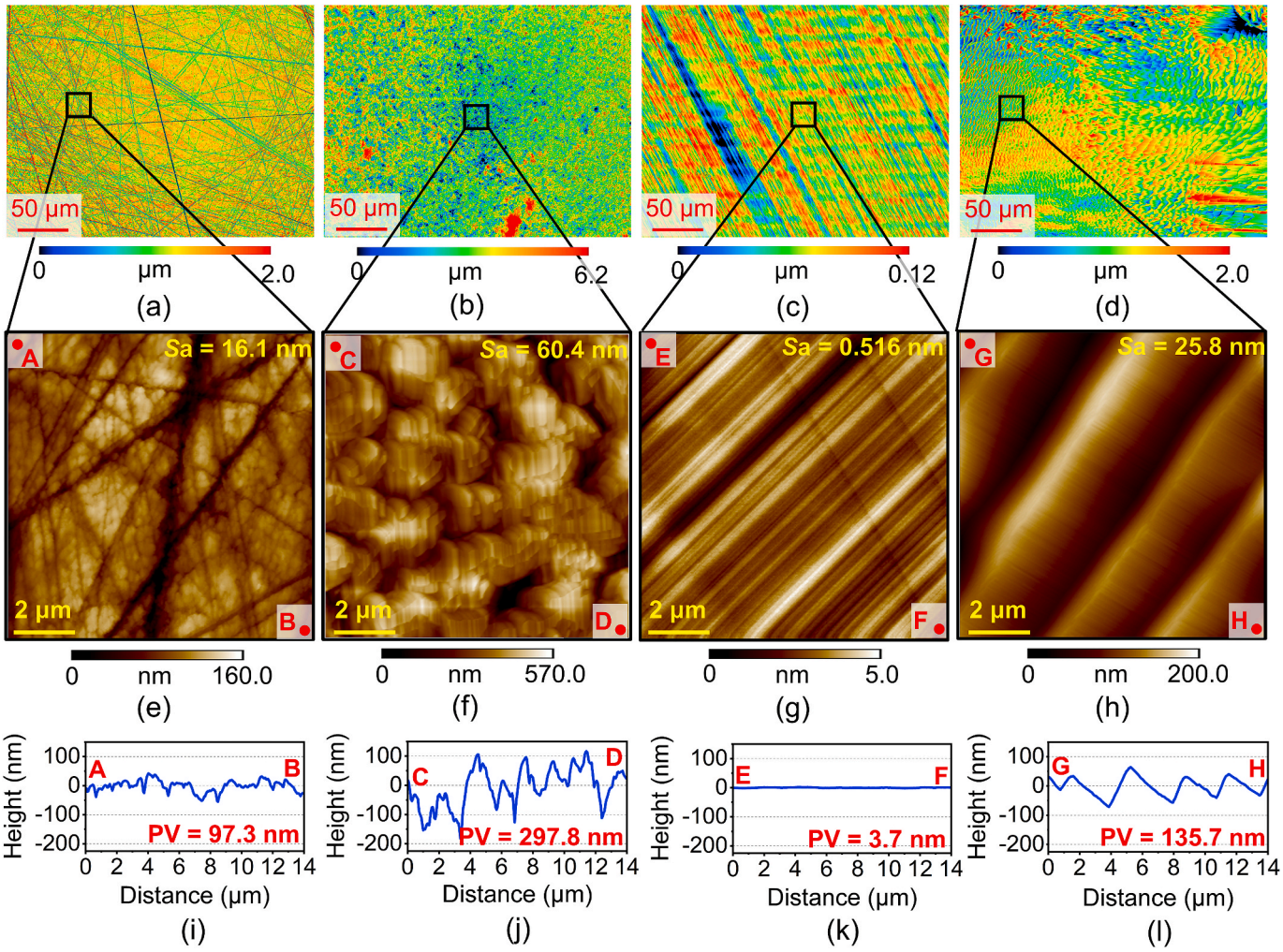

Fig. 4. Plasma-enabled atomic-scale reconstruction (PEAR) results of β-Ga_2O_3 (010) substrate at different radio frequency (RF) powers. Laser scanning confocal microscopy (LSCM) images of (a) as-received β-Ga_2O_3 and (b)–(d) PEAR-treated β-Ga_2O_3 at 700, 900, and 1100 W for 20 min, respectively. The corresponding (e)–(h) atomic force microscope (AFM) images and (i)–(l) profiles.

1100 °C; further increase in the RF power (to above 1000 W) leads to a temperature of approximately 1200 °C. This result shows that ICP plasma has a high temperature and its temperature can be controlled in a wide range. It should be noted that the energy required for surface reconstruction is different for different materials. This is why PEAR is expected to be applied to different TSOs. Next, we performed optical emission spectroscopy (OES) of the plasma at 900 W. As shown in Fig. 2b, most of the strong peaks originate from Ar. In addition, a relatively strong peak at 842.8 nm attributed to excited oxygen and two rather weak peaks related to nitrogen can be observed. These oxygen and nitrogen components can be attributed to the ambient air. The OES results demonstrate that the Ar plasma shows high-radical-density characteristics and that these particles, which slightly impinge on the substrate surface, can distinguish the PEAR from the conventional HTA method. More specifically, the plasma irradiates nearly perpendicular to the substrate and spreads outward along the center of the surface, and thus, the high-density particles may considerably prohibit the dissociation of β-Ga_2O_3 in the vertical direction to the surface but promote the migration of surface atoms on the substrate, consequently leading to the highly-efficient surface reconstruction process in PEAR.

2.3. Plasma numerical simulations

Numerical simulations were conducted to explore the temperature and gas velocity distributions on the substrate during PEAR. The simulation details are presented in Section 2 of the supplementary information. Fig. 2c–e shows the simulated temperature distributions at 700, 900, and 1100 W, respectively. The temperature increases with an increasing RF power, which is consistent with the results displayed in Fig. 2a. The temperature distributions along a straight line from the center to the edge of the sample in the three aforementioned simulations are shown in Fig. 2i. These results indicate that the temperature distributions across the substrate surface are relatively uniform. Further, the gas velocity distributions at 700, 900, and 1100 W are depicted in Fig. 2f–h, respectively; the increase in RF power causes changes of the flow field. According to the velocity distribution results from the center to the edge of the sample, as shown in Fig. 2j, the velocity increases from the center to the edge. Thus, the Ar plasma can be regarded as a special complex field with the coupling of the thermal and flow fields.

2.4. Proposed PEAR

Owing to the high-temperature and high-particle-density features of Ar plasma, surface atoms can be induced to migrate under the high-energy plasma irradiation and the migration process would end with surface reconstruction. Based on this deduction, we conducted an experimental study and proposed the PEAR method, which is expected to be a novel atomic-scale technique for manufacturing TSOs. Fig. 3a presents a schematic diagram of the PEAR process for TSO wafers, and the micron-scale surface morphology diagrams before and after PEAR

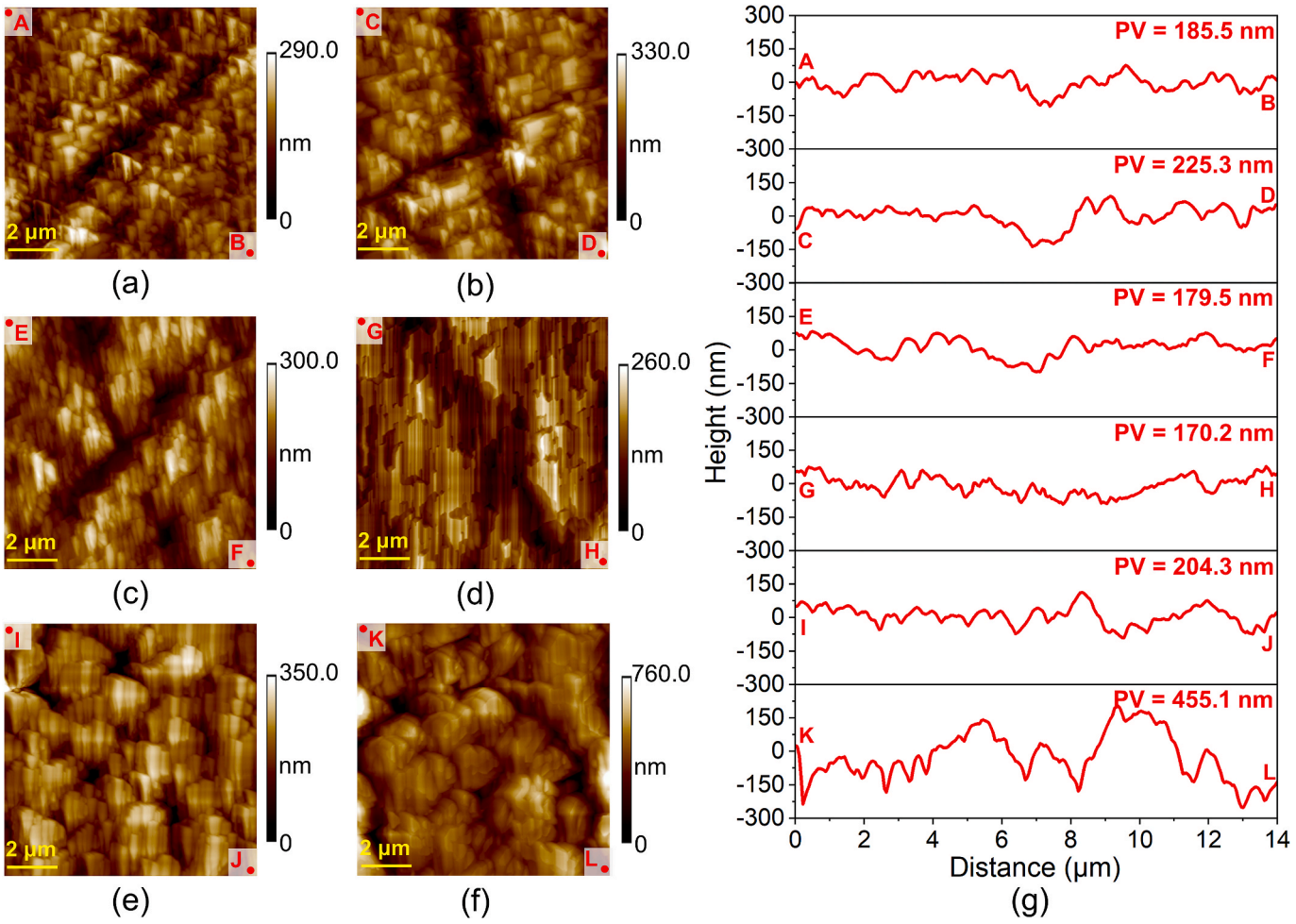

Fig. 5. Formation process of 2D-island β-Ga_2O_3 (010) surface at 700 W. (a)–(f) Atomic force microscope (AFM) images with different plasma durations. (a) 1, (b) 3, (c) 5, (d) 10, (e) 15, and (f) 20 min. (g) Corresponding profiles.

are shown in Fig. 3b. Scratches and peak-valley structures are observed on the original surface; however, the PEAR treatment dramatically converts this damaged and rough surface to an ultrasmooth surface with atomic step-terrace structures. The changes of the surface at the atomic-scale before and after PEAR are shown in Fig. 3c. For the as-received severely damaged surface, an amorphous layer and a subsurface damage layer exist above the single-crystal bulk. In the PEAR process, there are three types of reconstruction behaviors from the bulk to the surface. The subsurface damage layer recovers, the amorphous layer recrystallizes, and the rough surface forms a well-ordered atomic step-terrace structure. We infer that five steps, namely, dissociation, transportation, readsorption, migration, and rebonding, might occur during the formation of step-terrace structure, as shown in Fig. 3d [20,21].

3. Results

3.1. Effect of RF power on β-Ga_2O_3 (010) surface structure

The input RF power significantly affects the properties of the plasma, resulting in different surface reconstruction processes. Details of the materials and characterizations are provided in Section 3 of the supplementary information. Fig. 4 shows the PEAR results for different RF powers. We start with a damaged β-Ga_2O_3 (010) substrate. Remarkable scratches can be observed on the original surface, as shown in the laser scanning confocal microscopy (LSCM) image (Fig. 4a) and atomic force microscope (AFM) image (Fig. 4e). The corresponding *Sa* roughness is as high as 16.1 nm. In addition, the profile shown in Fig. 4i reveals that the peak-to-valley (PV) value is 97.3 nm. After 20-min PEAR treatment at 700 W, 2D-island structures can be found on the surface, resulting in an increase in the *Sa* roughness and PV values to 60.4 and 297.8 nm, respectively, as shown in Fig. 4b,f,j. Intriguingly, when the RF power increases to 900 W, the rough β-Ga_2O_3 substrate is converted to a smooth surface with *Sa* roughness of only 0.516 nm and a PV value of 3.7 nm, and atomic-scale step-terrace structures can be found on the surface, as shown in Fig. 4c,g,k. At 1100 W, the surface presents large step-terrace structures at the micron scale, and the corresponding *Sa* roughness and PV values are 25.8 and 135.7 nm, respectively, as shown in Fig. 4d,h,l. Hence, the reconstruction-induced structures on β-Ga_2O_3 are strongly determined on the basis of the RF power. Based on the morphology of the structures formed at 700, 900, and 1000 W, we name the corresponding PEAR processes as 2D-island, step-flow, and step-bunching modes, respectively.

3.2. Formation process of surface structures at different RF powers

The detailed formation processes of the three aforementioned structure types are discussed in this section. At 700 W, scratches can still be found on the surface at the beginning of PEAR and distinct bulges are formed, as shown in Fig. 5a–c. After 10 min, most of the scratches are healed (Fig. 5d) and the 2D-island structures are formed (Fig. 5e,f). Fig. 5g shows the changes in the profiles during the 2D-island migration. Compared with the as-received profile (shown in Fig. 4e), the PV first increases after irradiation with pure Ar plasma for the first 3 min; then, it decreases with the repair of scratches (from 3 to 10 min); finally, it

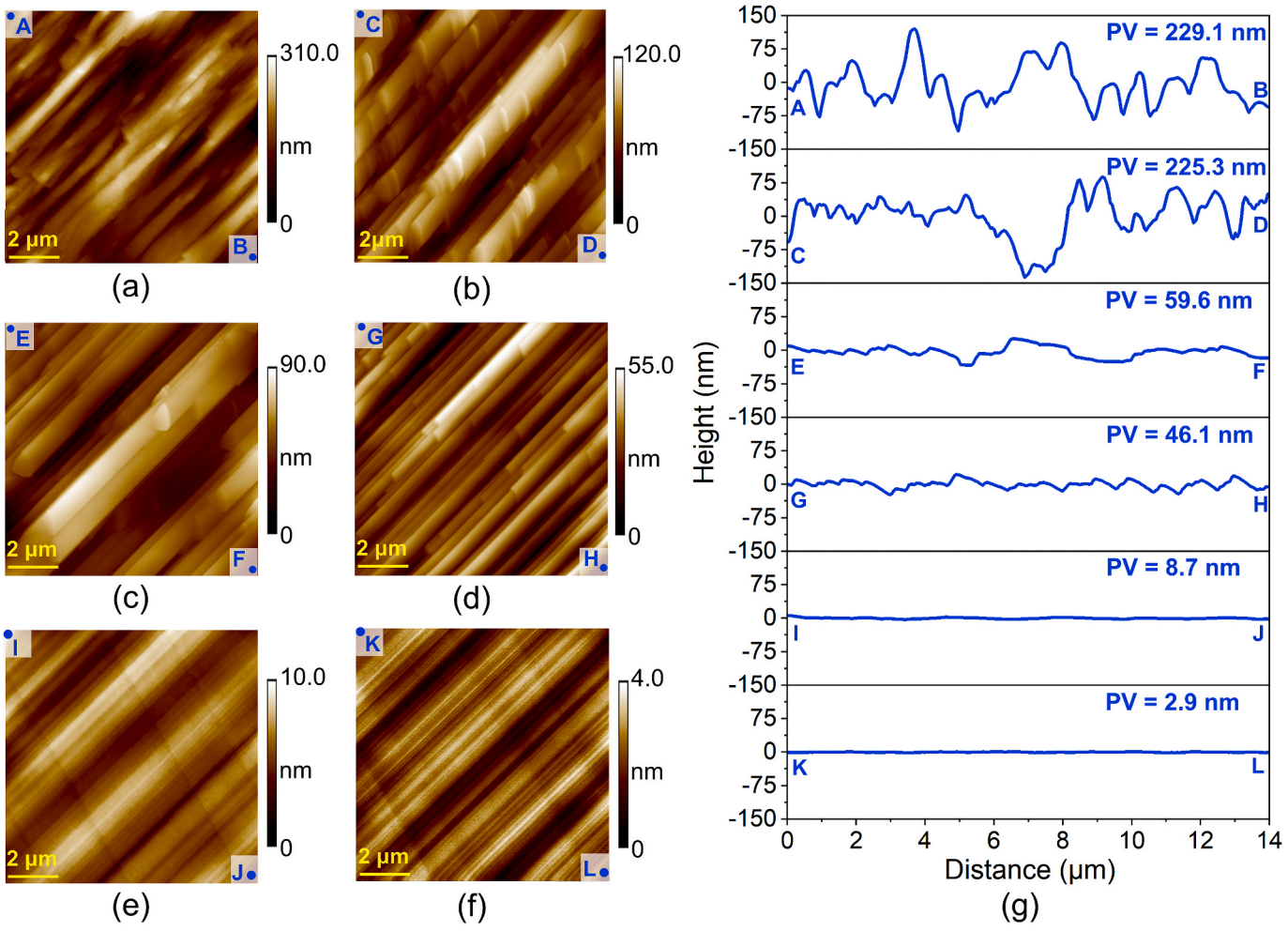

Fig. 6. Formation process of step-flow β-Ga_2O_3 (010) surface at 900 W. (a)–(f) Atomic force microscope (AFM) images with different plasma durations. (a) 1, (b) 3, (c) 5, (d) 10, (e) 15, and (f) 20 min. (g) Corresponding profiles.

increases with the formation of 2D-island structures (from 10 to 20 min). The final 2D-island surface shows a PV value of 455.1 nm, which is larger than that of the original profile, demonstrating the roughening effect of PEAR in the 2D-island mode.

Fig. 6 shows the formation process of the atomic-scale smooth β-Ga_2O_3 (010) surface. As depicted in Fig. 6a, a short plasma duration can efficiently heal scratches but leads to the appearance of step-like protrusions. These protrusions gradually evolve into step-terrace structures as the migration process progresses from 1 to 10 min, and the corresponding PV value continuously decreases, as can be seen in Fig. 6b–d,g. Significantly, many atomic-scale step-like structures exist on the surface (Fig. 6d); however, this surface is not ultrasmooth owing to the large surface undulation. Further prolongation of the PEAR duration to 15 and 20 min leads to an emphatic decrease in the PV value, as shown in Fig. 6e–g. Specifically, remarkable atomic-scale step-terrace structures are observed on the smooth surface with a PV value of 2.9 nm, as shown in Fig. 6f. According to the aforementioned reconstruction process, the formation of the atomically smooth β-Ga_2O_3 surface at 900 W can be divided into two stages. The early plasma irradiation is to heal scratches (Fig. 6a,b); the later plasma irradiation is to decrease PV value and yield an ultrasmooth feature at the atomic scale (Fig. 6c–f). These two stages constitute the proposed step-flow mode.

The formation process of the step-bunching β-Ga_2O_3 (010) surface is shown in Fig. 7. Very similar to the two aforementioned modes, the short plasma duration can cause the roughening of β-Ga_2O_3 (Fig. 7a,g). Most notably, the surface in Fig. 7a shows not only the island-like but also the layered-structure features, similar to the results presented in Figs. 5f and 6b. Additionally, as shown in Fig. 7b, step-like structures, similar to those in Fig. 6d, are formed as the duration is extended to 3 min; after the 5-min treatment (Fig. 7c), the PV value decreases to 21.6 nm. Here, the appearance of island-like features indicates that the initial atomic migration at 1100 W occurs in the 2D-island mode, and the formation of step-like structures and the decrease in the PV value demonstrate that the mid-term treatment induces the step-flow mode. Subsequently, further prolongation of the PEAR duration stimulates the third migration mode, namely, the step-bunching mode. As shown in Fig. 7c–g, the induced atomic-scale step-terrace structures are gradually bunched to generate micron-scale step-terrace structures, during which the PV value incrementally increases. After the 20-min PEAR treatment, the width and height of the bunched steps are approximately 0.45 and 0.35 μm, respectively. Thus, the final stable migration mode at 1100 W should be the step-bunching mode, and the micron-scale step-terrace structures should be stabilized on the surface.

3.3. *Surface roughness and weight variations during PEAR*

The changes in the surface roughness and weight of β-Ga_2O_3 are two significant aspects for understanding the manufacturing features of PEAR. Fig. 8a shows *Sa* roughness variations during the three migration modes. One common result is that the *Sa* roughness of β-Ga_2O_3 increases during the initial stage of PEAR; however, the following variations show evident differences. In the 2D-island mode, a significant reduction in the

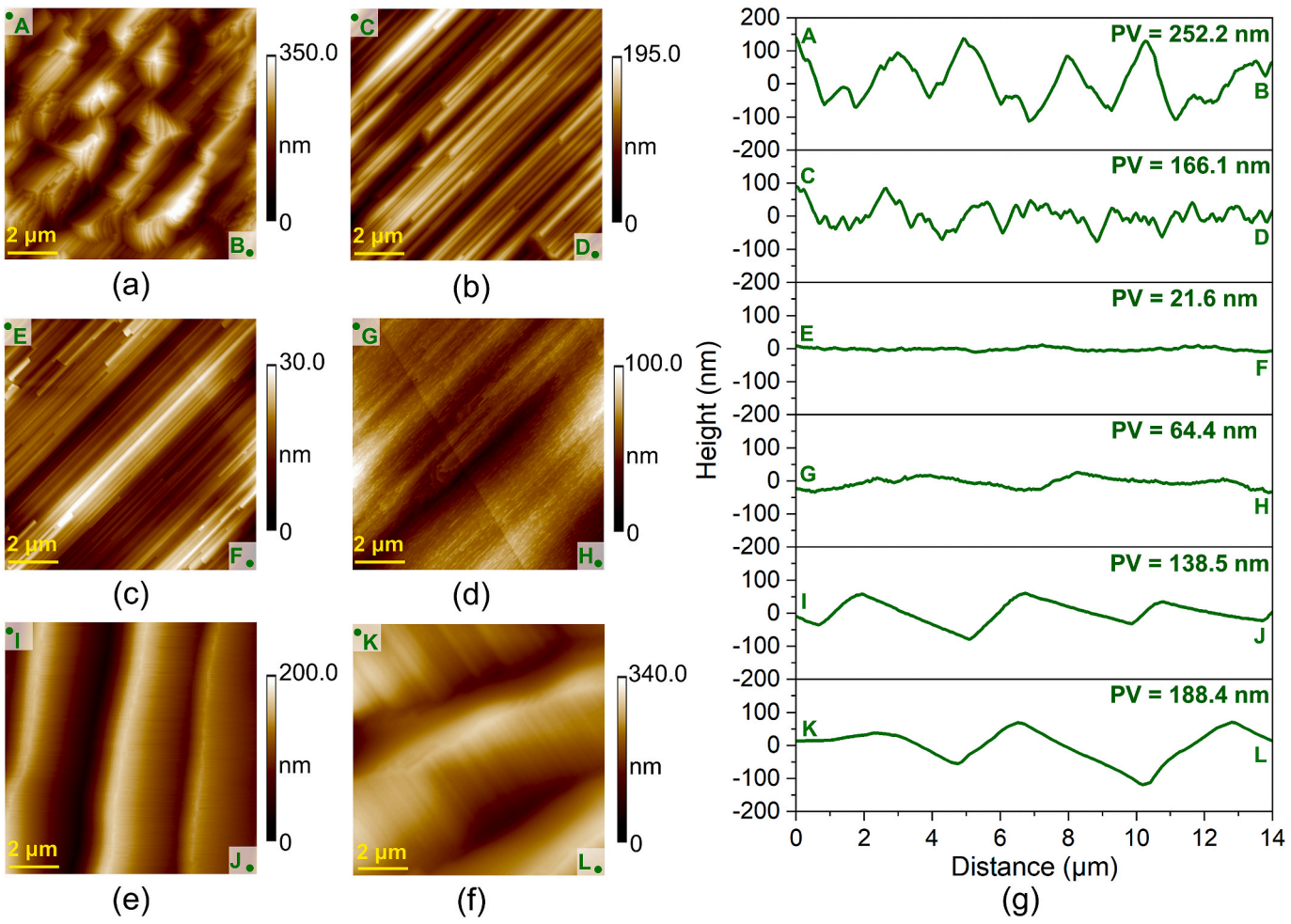

Fig. 7. Formation process of step-bunching β-Ga_2O_3 (010) surface at 1100 W. (a)–(f) Atomic force microscope (AFM) images with different plasma durations. (a) 1, (b) 3, (c) 5, (d) 10, (e) 15, and (f) 20 min. (g) Corresponding profiles.

Sa roughness is observed after the initial roughness increase, which can be attributed to the repair of scratches (Fig. 5b–d). Subsequently, the *Sa* roughness increases again, as the 2D-island structures are formed during this period. Compared with the as-received substrate, the 2D-island surface shows a relatively higher *Sa* roughness, which is caused by the kinetic roughening process [22,23]. In the step-flow mode, a successive *Sa* roughness reduction is observed when the plasma duration is longer than 1 min. During this period, atomic-scale step-like structures are first generated, followed by a flow of steps to decrease the PV value. In the step-bunching mode, after 1-min plasma treatment, the atomic-scale step-terrace structures are first formed, then flowed, and finally bunched, leading to an initial decrease and a subsequent increase in *Sa* roughness. According to the morphologies shown in Figs. 6 and 7 and the roughness variations in Fig. 8, we can find a close-to-2D-island surface in the step-flow mode and both a close-to-2D-island surface and a close-to-step-flow surface in the step-bunching mode. These results can help us understand the similarities and differences between the three modes.

Fig. 8b shows the weight variations of β-Ga_2O_3 during PEAR. The weight remains almost unchanged in the 2D-island mode, whereas it decreases slightly in both the step-flow and step-bunching modes. Here, we use the weight loss rate (WL%) variable to quantitatively evaluate the degree of weight change. The WL% is defined as:

$$WL\% = \frac{M - m}{M} \times 100\% \quad (1)$$

where M and m represent the weights before and after applying PEAR, respectively. The calculated WL% in the 2D-island, step-flow, and step-bunching modes are 0.026 %, 0.975 %, and 2.854 %, respectively. Rationally, the WL% in the 2D-island mode is close to zero, as the temperature is relatively low and the melting of the edges and corners of the sample can be almost ignored. However, in the step-flow and step-bunching modes, the experimental temperatures are above 1000 °C. Under these conditions, melting of the edges and corners becomes slightly significant owing to the thermal accumulation effect, consequently leading to a slight increase in the WL%. More importantly, we find that the maximum WL% in the step-flow and step-bunching modes always occur in the first 1 min of the plasma treatment. This indicates that the edges and corners of β-Ga_2O_3 are easier to melt; once the weak melting process is completed, the WL% in the following treatment should be small. Because the maximum WL% in the three aforementioned modes is only 2.854 %, we can reasonably claim that PEAR is an ultraprecision manufacturing method without material loss. To further demonstrate the no-material-removal feature of PEAR, we compared the WL% of four TSOs (β-Ga_2O_3, α-Al_2O_3, ZnO, and MgO) and obtained the corresponding optical images before and after PEAR, as shown in Section 4 of the supplementary information. These results can strongly demonstrate that the weight loss of β-Ga_2O_3 is due to the removal of cutting burrs (caused by the mechanical pre-cutting process) near the edges and corners of β-Ga_2O_3, and the weight changes of α-Al_2O_3, ZnO, and MgO are insignificant as no distinct burrs are generated during the pre-cutting process.

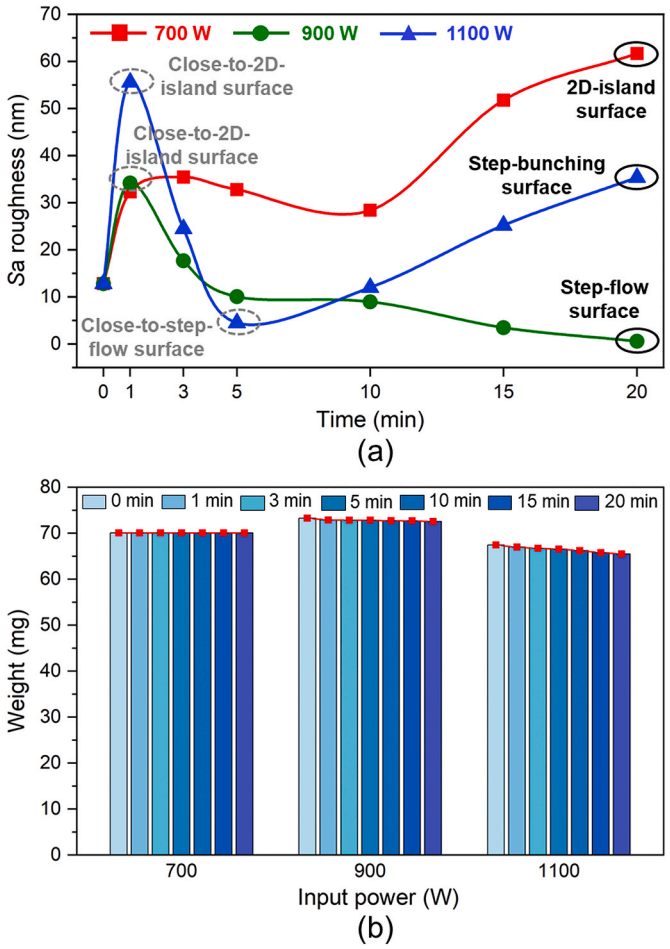

Fig. 8. Surface roughness and weight variations of β-Ga_2O_3 at 700, 900, and 1100 W. (a) *Sa* roughness. (b) Sample weight.

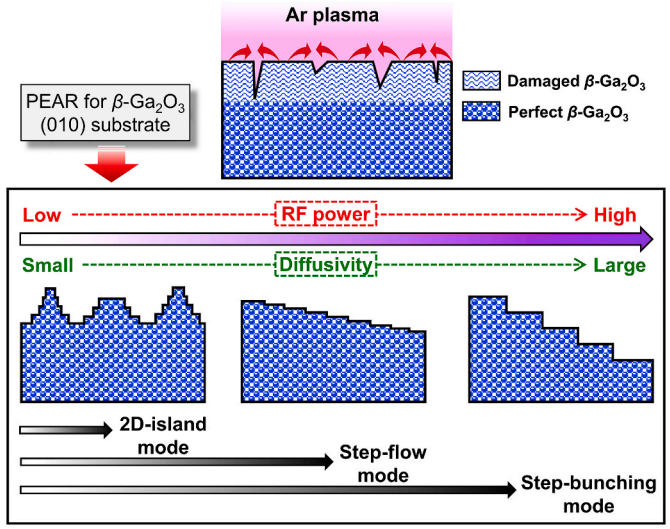

Fig. 9. A summary of plasma-enabled atomic-scale reconstruction (PEAR) of β-Ga_2O_3 (010) substrate.

3.4. Brief summary of PEAR of β-Ga_2O_3 (010) substrate

As discussed earlier, three migration modes, namely, 2D-island, step-flow, and step-bunching, are presented in the PEAR of β-Ga_2O_3. With an increase in the RF power, the final stable surface configurations in these modes should be rough surfaces with 2D islands, atomically smooth surfaces with step-terrace structures at the atomic scale, and relatively rough surfaces with micron-scale step-terrace structures, respectively, as shown in Fig. 9. Although the RF power determines the final stable surface configuration, a 2D-island period should exist before reaching the step-flow mode, and a 2D-island period and a step-flow period should be present before stabilizing in the step-bunching mode. Further, we infer that the diffusive behavior of atoms essentially molds the surface structures, as an increase in the RF power would definitely lead to an increasing in the diffusivity of atoms [24,25]. With small to large change in diffusivity, the final stable migration mode should be 2D-island, step-flow, and step-bunching, successively. To stabilize in any high-diffusivity mode, atoms must first pass through the corresponding low-diffusivity mode. However, at current stage, the transition RF power (or diffusivity) between two adjacent reconstruction modes has not been quantified because a small change in plasma power is difficult to be remarkably and quantitatively reflected in temperature and optical diagnosis.

Overall, the experimental results reveal three surface reconstruction modes of PEAR. It is not yet clear which surface reconstruction mode is most beneficial because it is closely related to subsequent wafer processes. However, there is no doubt that PEAR's three reconstruction modes also enrich its applicable scenarios.

3.5. Properties of PEAR-treated β-Ga_2O_3 (010) substrate

3.5.1. Surface integrity and crystalline quality

To investigate the properties of the β-Ga_2O_3 (010) surface after PEAR, we first conducted X-ray photoelectron spectroscopy (XPS) to study the surface integrity and determine whether any new element is introduced into the surface during PEAR. Here, we considered the step-flow surface as an example and compared its XPS result with the as-received β-Ga_2O_3. Fig. 10a shows the survey scan results of the two samples. Clearly, the two results are highly consistent, where only the peaks corresponding to Ga, O, and C are identified and C should originate from the C–H/C–O contaminants generated during XPS. Ar element cannot be detected on the surface, as shown in Fig. 10b. These results indicate that PEAR does not introduce additional elements into the surface. In addition, the XPS results of the Ga3d and O1s core levels in Fig. 10c,d indicate that no significant differences can be found before and after PEAR, demonstrating the pristine bonding nature of the β-Ga_2O_3 surface. Consequently, the surface integrity of β-Ga_2O_3 after PEAR can be guaranteed.

Next, we examined the crystalline quality of the β-Ga_2O_3 (010) surface with different structures by performing X-ray diffraction (XRD). As can be seen in Fig. 10e, the mechanical polishing-treated (MP-treated) β-Ga_2O_3 has a wide peak, indicating a certain degree of amorphous characteristics; by contrast, the CMP-treated β-Ga_2O_3 substrate shows a sharp peak, demonstrating its high crystalline quality. The PEAR-treated β-Ga_2O_3 substrates at different RF powers possess excellent crystallization characteristics as the corresponding peaks are quite sharp [26]. The full widths at half maximum (FWHM) of the five aforementioned peaks are displayed in Fig. 10f. The MP-treated β-Ga_2O_3 shows the largest FWHM of 0.577°, followed by the CMP-treated β-Ga_2O_3 with the FWHM of 0.110°. All PEAR-treated β-Ga_2O_3 substrates show a relatively small FWHM less than 0.1°, among which the step-flow β-Ga_2O_3 presents the smallest FWHM of 0.046°. It means that the crystalline quality of the surface processed by PEAR is even better than that of the CMP-treated substrate. These results indicate that PEAR is not only the rearrangement of the surface atoms, but also a reconstruction of the subsurface, thereby achieving improved crystalline quality. Additionally, the XRD peak of the step-flow β-Ga_2O_3 surface is located nearly at the same position as that of the CMP-treated β-Ga_2O_3 substrate, whereas the XRD peak of 2D-island surface slightly shifts to the lower diffraction angle side and that of step-bunching surface somewhat shifts to the higher

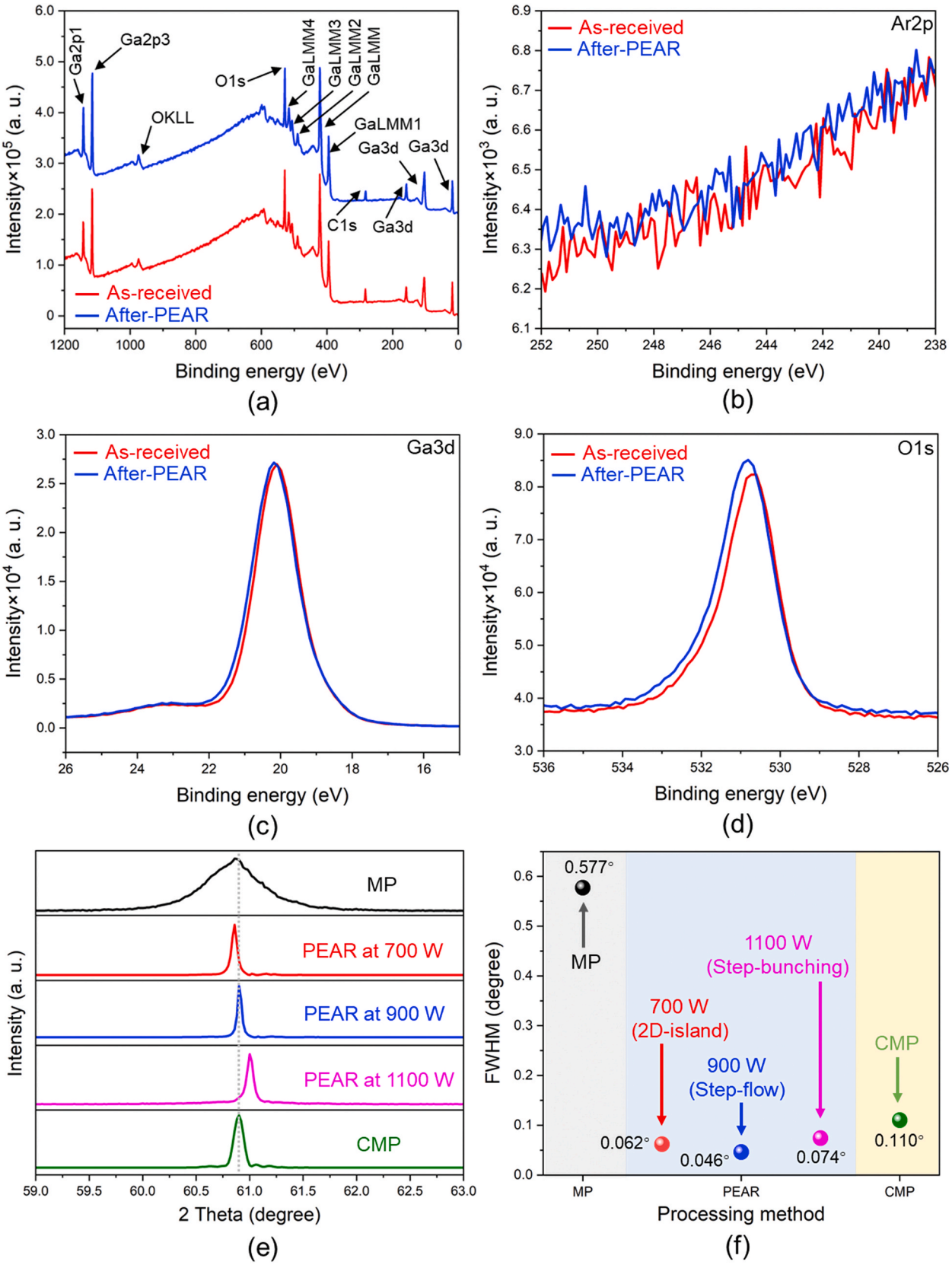

Fig. 10. Surface quality evaluations for β-Ga_2O_3 (010) substrates after plasma-enabled atomic-scale reconstruction (PEAR). (a)–(d) X-ray photoelectron spectroscopy (XPS) results: (a) survey scan, (b) Ar2p, (c) Ga3d, and (d) O1s. (e) and (f) X-ray diffraction (XRD) results: (e) XRD patterns and (f) full widths at half maximum (FWHM).

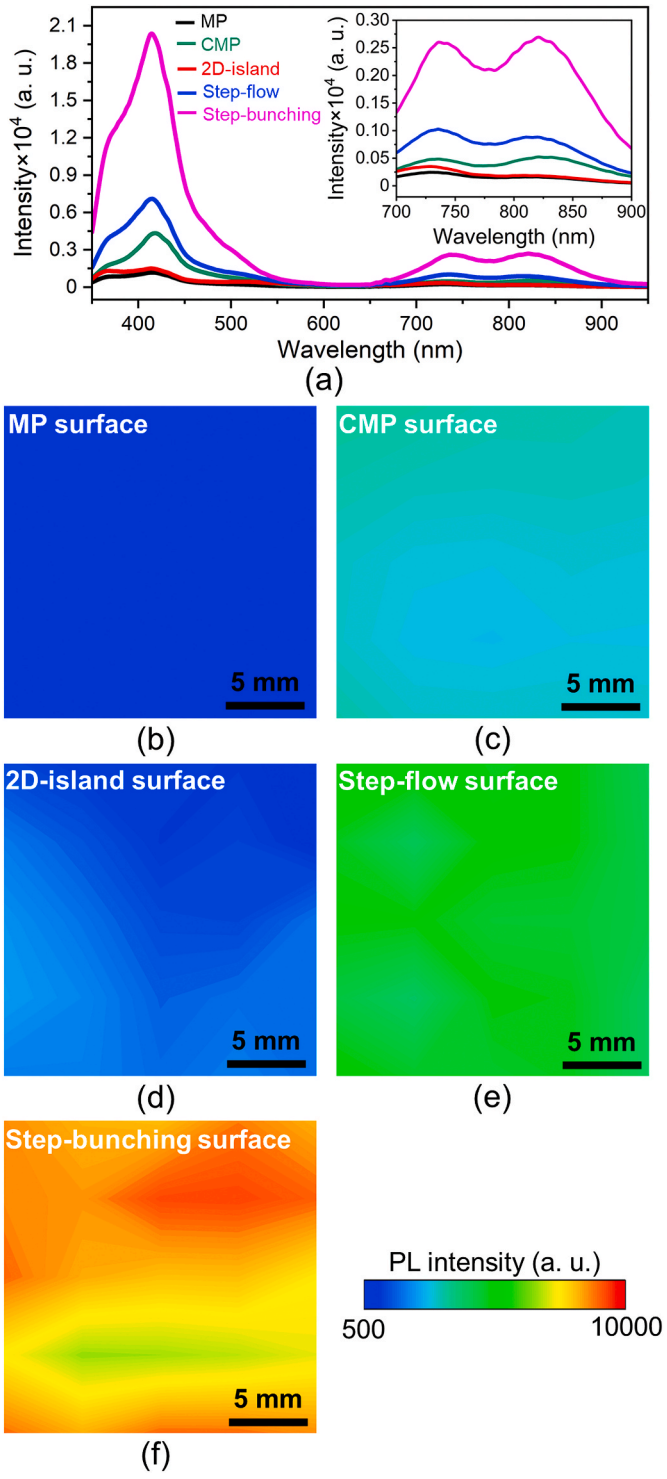

Fig. 11. Photoluminescence (PL) results of β-Ga_2O_3 (010) substrates. (a) Single-point PL spectra. 2D mapping results on (b) mechanical polishing (MP), (c) chemical mechanical polishing (CMP), (d) 2D-island, (e) step-flow, and (f) step-bunching surfaces, respectively.

diffraction angle side. A detailed explanation of the peak shifts can be found in Section 5 of the supplementary information. Therefore, the step-flow β-Ga_2O_3 with the atomic-scale smooth surface can be considered to possess the best crystallinity.

3.5.2. Photoelectric characteristic

As β-Ga_2O_3 can be utilized as a promising material for fabricating high-performance photoelectric devices, its photoelectric performance after PEAR must be investigated. Here, we compared the photoluminescence (PL) intensity of PEAR-, MP-, and CMP-treated β-Ga_2O_3, where all PL spectra were recorded by employing a confocal Raman spectroscope with a helium-cadmium (He–Cd) laser excitation source emitting at 325 nm. The single-point results in Fig. 11a depict that prominent PL peaks appear in the ranges of 350–500 and 700–900 nm, indicating the mid-ultraviolet, purple, blue, red, and infra-red emissions in the β-Ga_2O_3 substrates [27,28]. In both the two ranges, MP-treated β-Ga_2O_3 always shows the lowest PL intensity. Interestingly, the photoelectric performance of the 2D-island surface is slightly improved, as its intensity is slightly higher than that of MP-treated β-Ga_2O_3 but still much lower than that of CMP-treated β-Ga_2O_3. However, the step-flow and step-bunching surfaces exhibit considerably higher PL intensity, even compared with CMP-treated β-Ga_2O_3, and the bunched surface has the largest PL intensity among the five surfaces. The 2D mapping results in Fig. 11b–f, which are obtained based on the PL spectra in the range of 375–450 nm, reveal that the PL intensity distributions of the five substrates are relatively uniform. These results demonstrate that the PEAR treatment in the step-flow and step-bunching modes can greatly enhance the photoelectric property of β-Ga_2O_3 to better than that of CMP-treated β-Ga_2O_3. Especially, the smooth step-flow β-Ga_2O_3 may be directly used to fabricate novel β-Ga_2O_3-based photoelectric devices. A possible reason for this plasma-enhanced PL phenomenon is provided in Section 6 of the supplementary information.

3.5.3. Subsurface features at atomic scale

To confirm the ability of PEAR to smooth β-Ga_2O_3 and repair its subsurface damage layer, we conducted transmission electron microscopy (TEM) observation and evaluated the atomic-scale subsurface feature of the step-flow surface. Fig. 12a–c shows the cross sections of as-received β-Ga_2O_3 with obvious scratches. Clearly, the original surface is quite rough and many cracks in the subsurface damage layer can be observed (Fig. 12a). In Fig. 12b, some dislocations and a stress region can also be observed, and the selected-area electron diffraction (SAED) pattern indicates a certain degree of amorphous features. Additionally, an amorphous layer with a thickness of approximately 20 nm is observed on the surface (Fig. 12c). The aforementioned surface and subsurface defects are believed to be generated by the mechanical action during the lapping process [29,30].

In contrast, the step-flow surface presents a remarkable atomically smooth feature. As shown in Fig. 12d, the interface between the protective carbon layer and β-Ga_2O_3 is extremely flat and no cracks and dislocations can be found. A high-resolution TEM image of the interface is obtained, as shown in Fig. 12e. β-Ga_2O_3 after PEAR shows relatively clear and regular atomic arrangement, demonstrating its high crystalline quality. In addition, the improved crystallinity is proven by the clear single-crystal SAED pattern shown in Fig. 12f. The element distributions at the cross section of this step-flow substrate are shown in Fig. 12g–k. Conspicuously, only Ga and O elements can be detected in the substrate, which again strongly demonstrates that PEAR does not introduce any Ar element into β-Ga_2O_3. These results indicate that the subsurface damage layer was recovered and the amorphous layer was recrystallized. Therefore, via PEAR in the step-flow mode, a severely damaged β-Ga_2O_3 substrate can be directly transformed into a damage-free and atomically smooth surface without any material removal.

3.6. Comparison with common surface finishing methods

Generally, several methods, including CMP, WCE, and HTA, can be adopted to improve the surface quality of β-Ga_2O_3. Here, we compared PEAR with the aforementioned methods in terms of the optimized surface roughness and roughness reduction rate (V), where V is defined as

$$V = \frac{SR_0 - SR_1}{t} \quad (2)$$

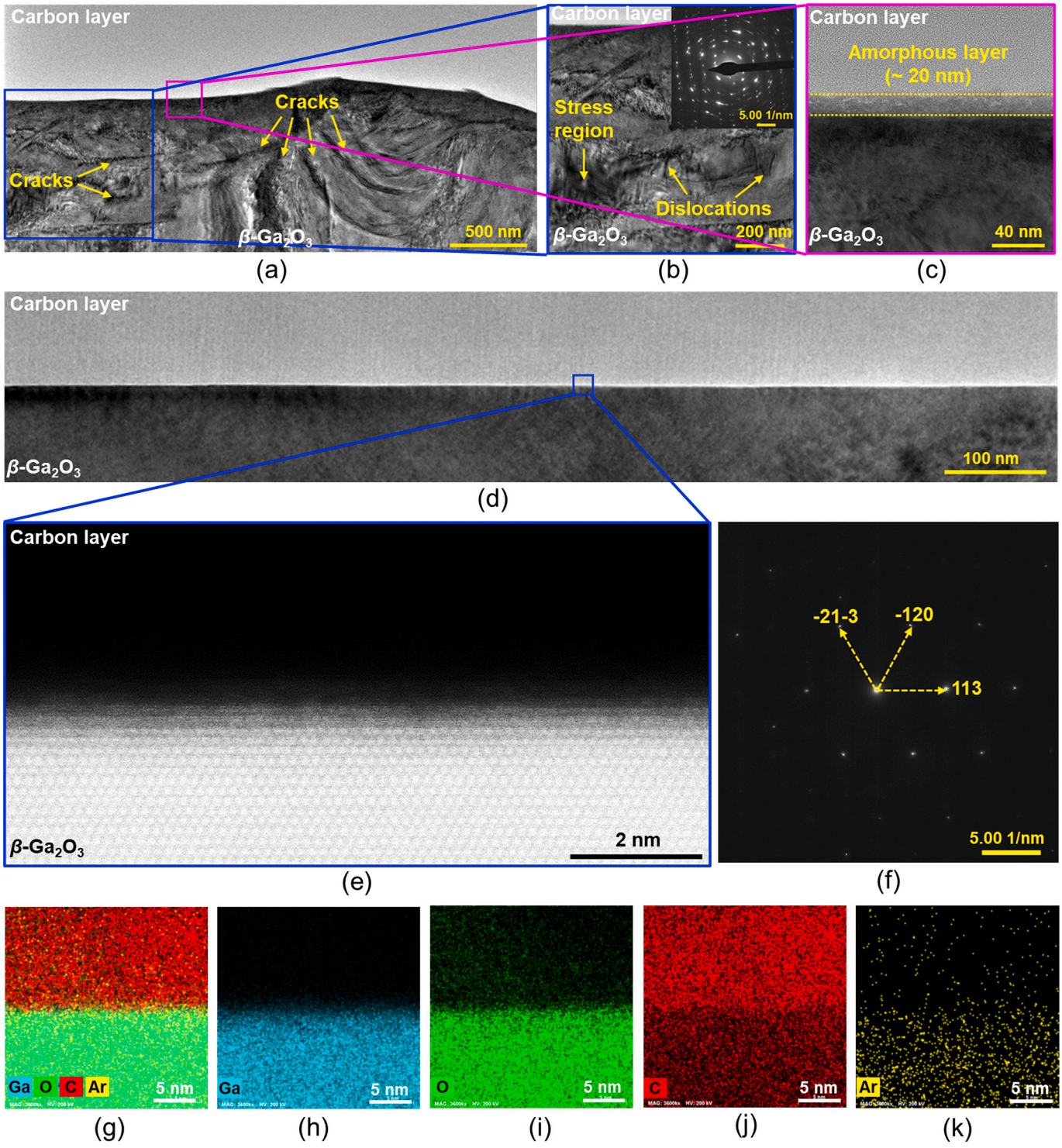

Fig. 12. Subsurface analyses of β-Ga_2O_3 (010) substrates before and after plasma-enabled atomic-scale reconstruction (PEAR). (a)–(c) Transmission electron microscopy (TEM) images of as-received β-Ga_2O_3. The inset in (b) is a selected-area electron diffraction (SAED) pattern obtained near cracks. (d) TEM image, (e) high-resolution TEM image, (f) SAED pattern, and (g)–(k) element mapping results of the step-flow β-Ga_2O_3.

where SR_0 and SR_1 represent the surface roughnesses before and after processing, respectively, and t is the experimental duration. Fig. 13a–c shows the schematic diagrams of CMP, WCE, and HTA for β-Ga_2O_3, respectively. Compared with the three existing methods, the PEAR exhibits at least the following characteristics (Fig. 13d). First, it can achieve the smallest surface roughness of 0.098 nm. Second, it shows a relatively large V (24.30 nm/h), demonstrating its high efficiency. Third, PEAR can be regarded as a typical process of material transfer on the surface, and no increase or decrease in material occurs during processing; this is known as equal manufacturing, which is a development direction in the manufacturing field, in addition to the conventional subtractive manufacturing [31] and novel additive manufacturing [32]. Therefore, PEAR has the potential to compete with or even surpass the existing manufacturing methods for β-Ga_2O_3.

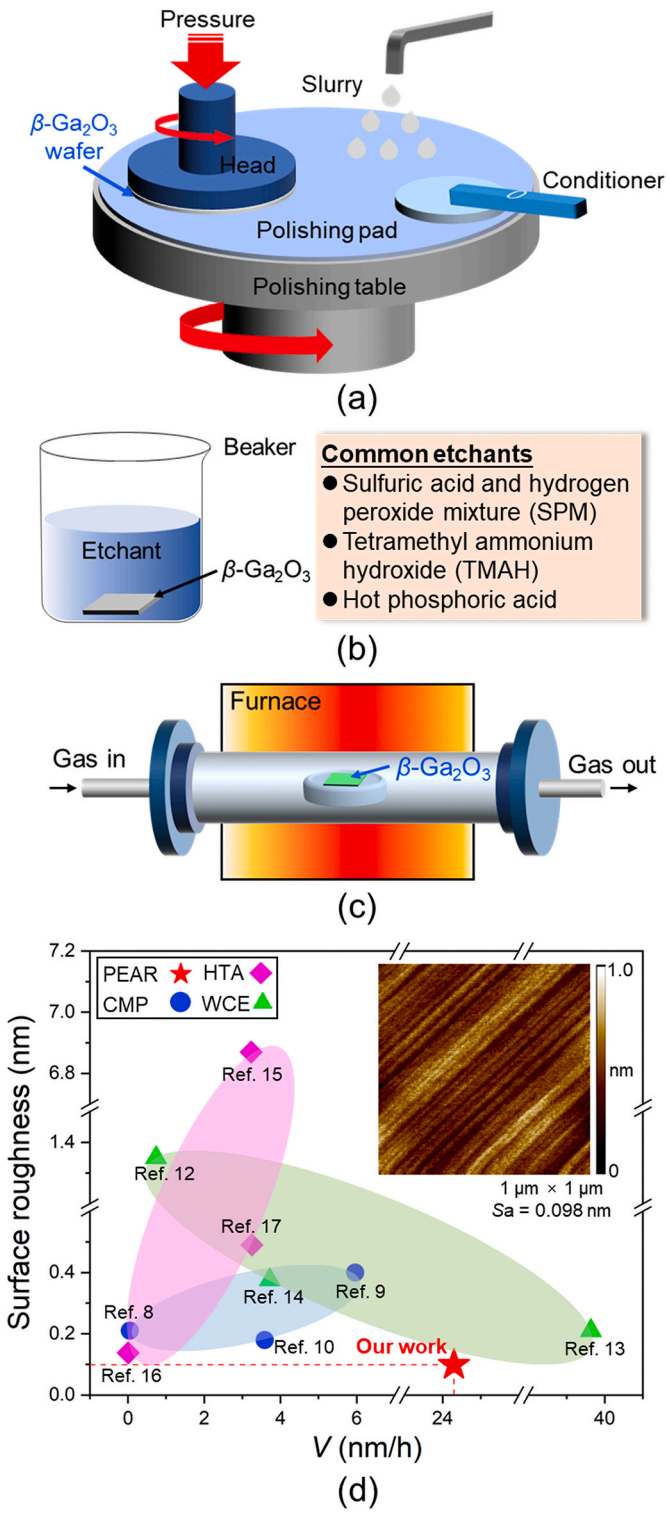

Fig. 13. Comparison of various surface finishing methods. Schematic diagrams of (a) chemical mechanical polishing (CMP), (b) wet chemical etching (WCE), and (c) high temperature annealing (HTA), respectively. (d) Statistical result about β-Ga_2O_3 processing. The inset is an atomic force microscope (AFM) image of the step-flow surface obtained via plasma-enabled atomic-scale reconstruction (PEAR).

3.7. Promotion of PEAR

3.7.1. PEAR for β-Ga_2O_3 substrates with other crystal faces

PEAR has been proven to be able to smooth the β-Ga_2O_3 (010) substrate through the step-flow mode. We extended PEAR to polish other crystal faces of β-Ga_2O_3. Fig. 14 shows the surface morphologies of the β-Ga_2O_3 (−201), (100), and (001) substrates before and after PEAR. Conspicuous scratches are observed on the original surfaces, as shown in Fig. 14a–c. These surfaces exhibit large *Sa* roughness of 26.7, 39.3, and 14.0 nm, respectively. After the 20-min PEAR at 900 W, these surfaces are polished to atomic-scale smooth states with *Sa* roughnesses of 0.286, 0.057, and 0.263 nm, as shown in Fig. 14d–f, respectively, demonstrating that these surfaces also go through the step-flow mode. Notably, the surface roughness change in the β-Ga_2O_3 (100) substrate is the most significant, which may indicate that the step-flow phenomenon is more significant for the atoms on the (100) surface than for those on other surfaces. These results strongly demonstrate that the smoothing effect of PEAR method is independent of the crystal faces of β-Ga_2O_3.

3.7.2. PEAR for α-Al_2O_3 (0001), ZnO (000–1), and MgO (100) substrates

To explore the generality of PEAR for fabricating atomically smooth and damage-free surface, we utilized it to process several other wide-bandgap TSOs, namely, α-Al_2O_3 (0001), ZnO (000–1), and MgO (100) substrates. More information about these three materials and the PEAR details can be found in Section 7 of the supplementary information. Fig. 15a shows the atomic structure of α-Al_2O_3, where the (0001) surface terminated by Al atoms is represented as a green plane. A damaged α-Al_2O_3 substrate with *Sa* roughness of 1.42 nm is adopted as the as-received surface, as shown in Fig. 15b. After PEAR at 600 W for 5 min, a smooth α-Al_2O_3 substrate with *Sa* roughness of 0.077 nm can be obtained, and atomic-scale step-terrace structures can be observed on it, as shown in Fig. 15c. The HR-TEM image in Fig. 15d confirms that no missing or extra atoms at the terrace, and the step height is approximately 0.50 nm, which is consistent with the height of bilayer α-Al_2O_3. Similar processing results are also obtained for ZnO and MgO substrates. As shown in Fig. 15e–h, a smooth ZnO surface (*Sa* = 0.073 nm) can be achieved after PEAR at 600 W for 10 min, and the width and height of the uniform ZnO step-terrace structure are evaluated to be approximately 240 and 0.5 nm, respectively, thereby demonstrating that the step consists of two layers of ZnO atoms as the interplanar distance of ZnO is approximately 0.26 nm. Fig. 15i-l presents the PEAR results of MgO at 600 W for 10 min. Clearly, the *Sa* roughness is dramatically reduced from 1.87 to 0.070 nm, and the atomic-scale step, consisting of two layers of MgO, can be identified. Obviously, the smooth step-terrace β-Ga_2O_3 (with different crystal faces), α-Al_2O_3, ZnO, and MgO surfaces were achieved via PEAR. These results strongly demonstrate that the PEAR process is a general approach for atomic surface manufacturing towards various TSOs.

4. Discussion

4.1. Mechanism of PEAR

4.1.1. Energy barrier for the migration of surface atoms

To understand the PEAR mechanism, we first performed density functional theory (DFT) based calculations to reveal the migration ability of the surface atoms on β-Ga_2O_3. Details of the model and calculations are provided in Section 8 of the supplementary information. Fig. 16a,b presents the top and side views of the migration path of Ga, respectively. At the initial state (IS), the Ga atom is located at the "bridge" site between two oxygen (O) atoms; at the final state (FS), the Ga atom is anchored by three O atoms to form a perfect β-Ga_2O_3 (010) face. The energy profile shown in Fig. 16c indicates that two transition states (TSs), TS1 and TS2, can be found during the migration process, and the corresponding energy barriers (E_a) are 0.46 and 0.29 eV, respectively. The Ga atoms at TS1 and TS2 are bonded at the "bridge" site between adjacent Ga and O atoms, and the vibration spectrum analysis demonstrates that TS1 and TS2 are true TSs as both states possess only one imaginary frequency. Hence, the energy barrier for the aforementioned migration process should be only 0.46 eV, indicating

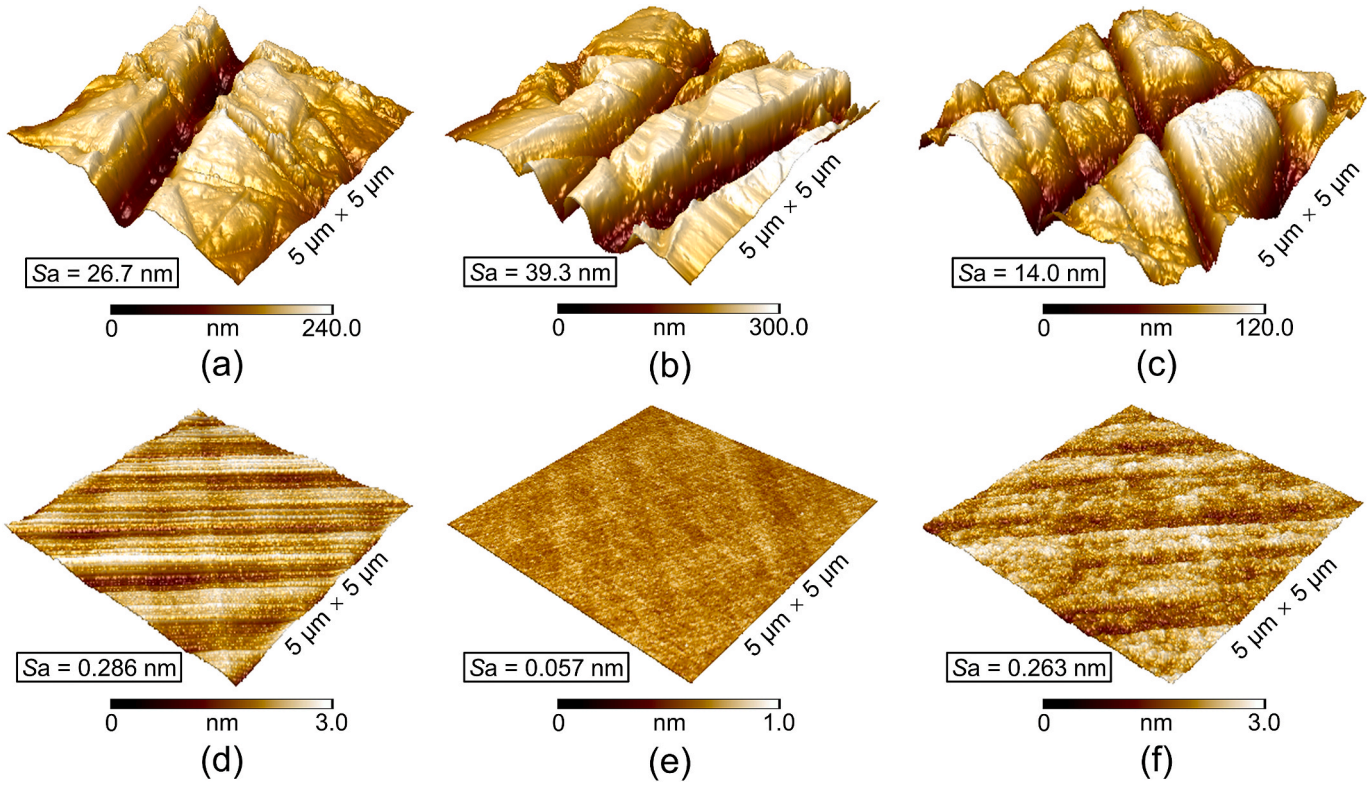

Fig. 14. Atomic force microscope (AFM) images of β-Ga_2O_3 substrates with various crystal faces. (a) (−201), (b) (100), and (c) (001) before plasma-enabled atomic-scale reconstruction (PEAR). (d) (−201), (e) (100), and (f) (001) after PEAR at 900 W for 20 min.

that the atom migration effect is expected to be achieved above the room temperature (R_T). The small migration energy should be easily overcome, as atoms can gain enough energy from the plasma with high-temperature and high-radical-density features. Once irradiated by the plasma, atoms would be activated to migrate until they are anchored. This is why PEAR can be achieved in the experiment. Here, we only consider the migration process of Ga atoms, and the O atom is believed to migrate more easily on the surface because the atomic mass of O is much less than that of Ga [33].

Because the migration of Ga atoms is essentially a surface diffusion process at a certain temperature, we adopted diffusivity (D) to quantitatively describe the relationship between migration and temperature. We express D as

$$D = D_0 \exp\left(-\frac{E_a}{k_B T}\right) \tag{3}$$

where D_0 is the pre-exponential factor, E_a is the energy barrier, k_B is the Boltzmann constant ($k_B = 1.381 \times 10^{-23}$ J/K), and T is the temperature [34,35]. As E_a is calculated to be 0.46 eV, we plot the $\frac{D}{D_0}$ *vs.* T curve, as shown in Fig. 16d. Evidently, the diffusivity of the Ga atoms increases exponentially with an increase in temperature. We further calculated the relative diffusivity ratios at 600, 800, 1000, 1200, and 1400 K and compared them with the diffusivity at 300 K; the results are shown in Fig. 16e. Significantly, the diffusivity at 600 K is more than seven thousand times that at 300 K. When the temperature reaches 1000 K, the ratio is 2.56×10^5. At 1400 K, the diffusivity ratio exceeds one million. The change in migration modes and the formation of different structures might be attributable to the remarkable increase in diffusivity with the RF power in the experiments [25].

4.1.2. Migration and reconstruction process

We conducted classical large-scale molecular dynamics simulations to catch the detailed atoms' migration and reconstruction behavior, in which the high-temperature and high-density-particle features of the plasma were considered [33]. We first established a small model (24.55 × 100 × 23.85 Å^3) with 1024 Ga atoms, 1536 O atoms, and 100 Ar atoms to explore the diffusion processes under different conditions. The calculation details and discussions are provided in Section 9 of the supplementary information. PEAR treatments in 2D-island, step-flow, and step-bunching modes can promote the amorphous-to-crystal transformation of β-Ga_2O_3, which is consistent with the experimental XRD results. In addition, increasing the RF power of the plasma can accelerate the motion of the atoms, and the motion of the O atoms should always be faster than that of the Ga atoms.

We further built a large model to study the detailed diffusion and crystallization process of β-Ga_2O_3 under the step-flow condition, as a promising atomic-scale smooth β-Ga_2O_3 surface can be found in the corresponding experimental situation. The left panel of Fig. 17a shows the configuration of the original model having the size of 98.21 × 100 × 95.39 Å^3 and 15,383 Ga atoms, 23,093 O atoms, and 1600 Ar atoms. The model can be divided into three parts, namely, single-crystal β-Ga_2O_3, amorphous β-Ga_2O_3, and pure Ar plasma, along the <010> direction. The enlarged inset shows the atomic arrangement of the amorphous layer, where both the Ga and O atoms exhibit significantly disordered distributions. Four hemispherical pits with a diameter of 30 Å are created and evenly distributed on the surface of the model, to simulate a rough surface. As depicted in the middle panel of Fig. 17a, the amorphous β-Ga_2O_3 layer converts to crystal after 10 ns simulation under the condition of T = 1081 °C and ρ = 4.77 eV/nm^2 (note that T is the experimentally measured temperature and ρ is the energy density of plasma); the relatively regular arrangement of O and Ga atoms can be clearly observed in the corresponding inset. The crystallinity can be further improved after quenching to R_T at the rate of 1 °C/ps, as illustrated in the right panel of Fig. 17a. The dynamic isothermal processes from the side (along <001> direction) and top (along <0–10> direction) views are displayed in supplementary Videos 2 and 3, respectively. The dynamic quenching processes from the two views are presented in

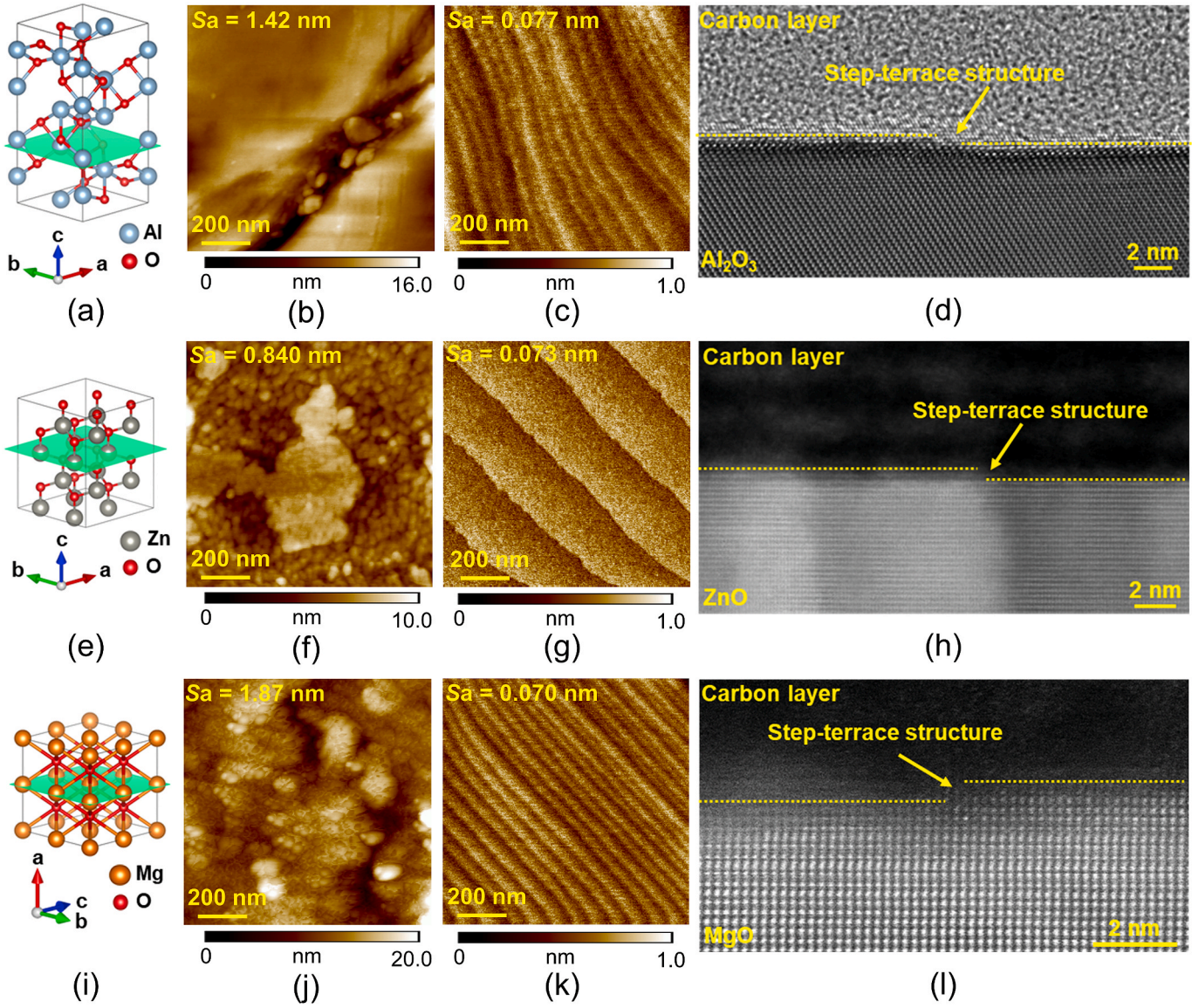

Fig. 15. Plasma-enabled atomic-scale reconstruction (PEAR) results of α-Al_2O_3 (0001), ZnO (000–1), and MgO (100) substrates. Atomic structures of (a) α-Al_2O_3, (e) ZnO, and (i) MgO, where the green planes indicate the corresponding (0001), (000–1), and (100) surfaces, respectively. Atomic force microscope (AFM) images of (b) α-Al_2O_3, (f) ZnO, and (j) MgO before PEAR and (c) α-Al_2O_3, (g) ZnO, and (k) MgO after PEAR. High-resolution transmission electron microscopy (TEM) images of PEAR-treated (d) α-Al_2O_3, (h) ZnO, and (l) MgO. (For interpretation of the references to colour in this figure legend, the reader is referred to the Web version of this article.)

Supplementary Videos 4 and 5, respectively.

Supplementary video related to this article can be found at https://doi.org/10.1016/j.ijmachtools.2024.104119

The detailed diffusion and crystallization processes are shown in Fig. 17b–e. During the initial 1 ns of diffusion, fast crystallization is observed along the <010> direction (Fig. 17b). From 1 to 2 ns, the crystallization of atoms along <010> direction slows down, but the gradual regular arrangement of atoms along the <010> direction can still be observed (Fig. 17c). In the subsequent motion process, the crystallization mainly expands in the (010) plane, as shown in Fig. 17d, e. These three crystallization stages can also be numerically illustrated in the mean square displacement (MSD) results along the <100>, <010>, and <100> directions, as shown in Fig. 17f–h, respectively. In stage 1 (0–1 ns), the MSD in all three directions prominently increases with the simulation time, but the crystallization in the <010> direction is the most significant. In stage 2 (1–2 ns), the rate of increase in the MSD in the <100> and <001> directions is gradually reduced, indicating that the diffusion of surface atoms in these two directions becomes weaker; in particular, the MSD in the <010> direction tends to remain unchanged, demonstrating a relatively stable crystalline state. In stage 3 (2–10 ns), the rate of increase in the MSD in <100> and <001> directions stabilizes at constant values, and no significant displacement can be observed in the <010> direction. Under this condition, the crystallization process mainly extends towards the <100> and <001> directions. As per the diffusion processes described earlier, the amorphous layer on the surface rapidly transforms into a crystalline layer. Clearly, these detailed behaviors of Ga and O atoms at nanoscale should be the essence of PEAR. The results provide evidence to understand the atoms' reconstruction process during PEAR and the improved crystalline quality after PEAR. However, note that the top few layers of atoms still do not exhibit a perfect arrangement, which may be attributed to the spontaneous atomic thermal motion at R_T.

In addition to the crystallization phenomenon caused by diffusion, we studied the surface morphological changes during the simulation of the step-flow mode. Fig. 18a shows the top view of the model in the <0–10> direction. Fig. 18b shows the corresponding sectional view

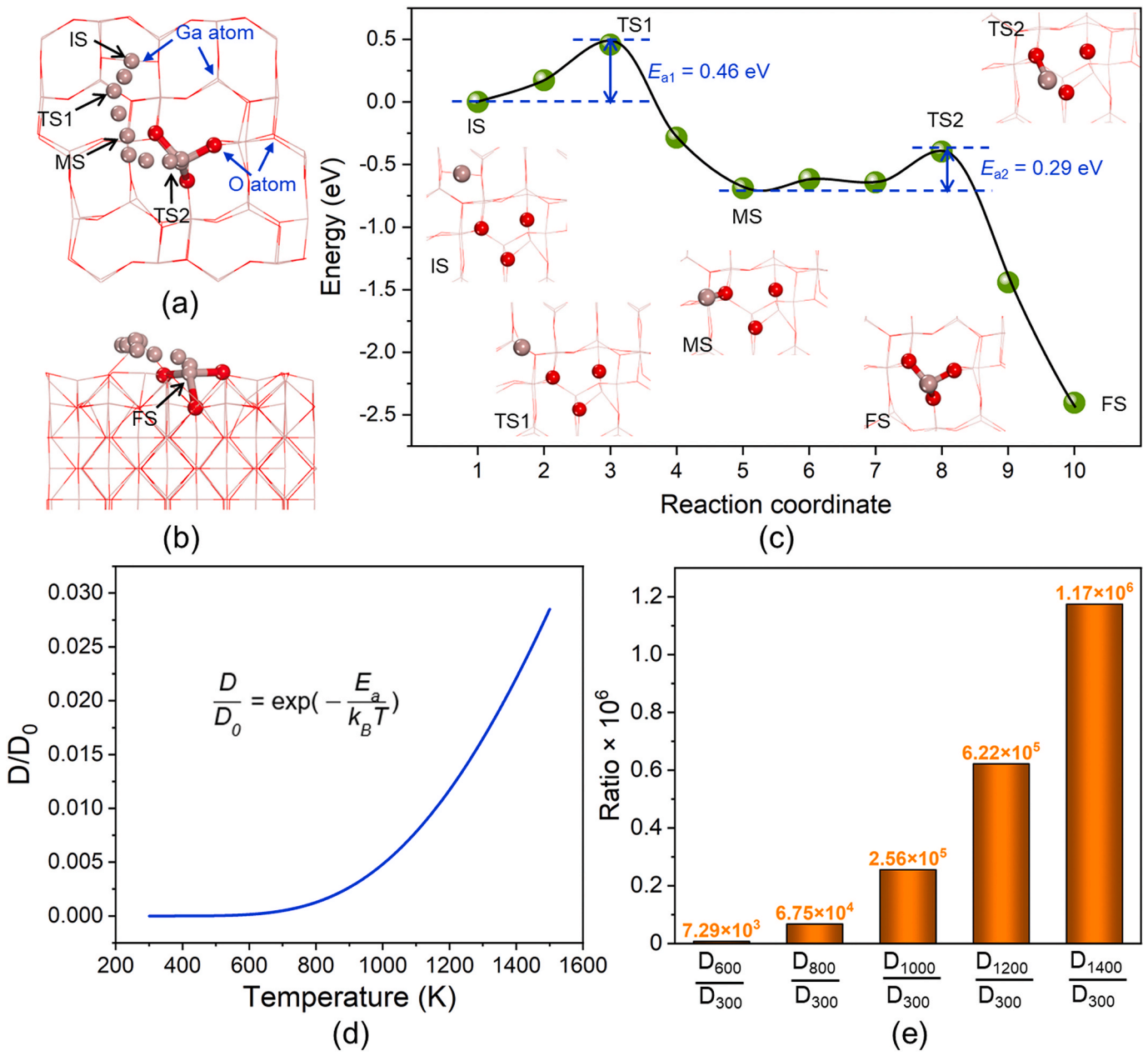

Fig. 16. Density functional theory (DFT) based calculations for the migration of Ga atom on β-Ga_2O_3 (010) substrate. (a) Top and (b) side views of the migration process. (c) Energy profile of the migration process. The insets are the corresponding atomic structure configurations. (d) Relative diffusivity variation of Ga atom with temperature. (e) Ratio of diffusivity at different temperatures to that at 300 K.

along the <001> direction, and the blue line in Fig. 18a indicates the position of the section. As the atomic migration process proceeds, the hemispherical pits are gradually filled, the degree of crystallization is gradually enhanced, and the surface height fluctuation progressively decreases. Additionally, a significant decrease in the potential energy per atom is observed during the initial 2 ns (Fig. 18c). After 2 ns, the potential energy of the system tends to stabilize at approximately −5.71 eV/atom, indicating that the system has reached a relatively stable state.

Fig. 18d shows the changes in the *Sa* roughness and number of surface atoms (N_{surf}) during the simulation, and the insets display the corresponding surface models at different times. *Sa* roughness decreases from 0.433 to 0.150 nm within only 1 ns, accompanied by a decrease in N_{surf} from 1273 to 808. Subsequently, the reductions in *Sa* roughness and N_{surf} are not significant. At 10 ns, the values of *Sa* roughness and N_{surf} are calculated to be 0.122 nm and 771, respectively. Thus, it can be claimed that the step-flow mode can lead to the atomically smooth surface because of plasma-induced fast diffusion and reconstruction. In particular, the 2D-island and step-bunching structures observed in the experiments cannot be found in the nanoscale MD simulations, owing to their overlarge dimensional features at the micron scale. Fig. 18e shows the radial distribution function (RDF) of Ga–O before and after reconstruction. In comparison, after the reconstruction process, all peaks are stronger and narrower; the nearly zero valleys between the first and second peaks and between the third and fourth peaks can be observed; the fourth peak near 5.5 Å can only be found in the structure after reconstruction. These RDF results again demonstrate the relatively good crystalline quality of β-Ga_2O_3 after PEAR [36].

4.1.3. *Coupling of thermal and flow fields in PEAR*

Compared with conventional HTA methods involving only the thermal field, the PEAR combines the thermal and flow fields together. Here, we conducted finite element analyses to illustrate the difference

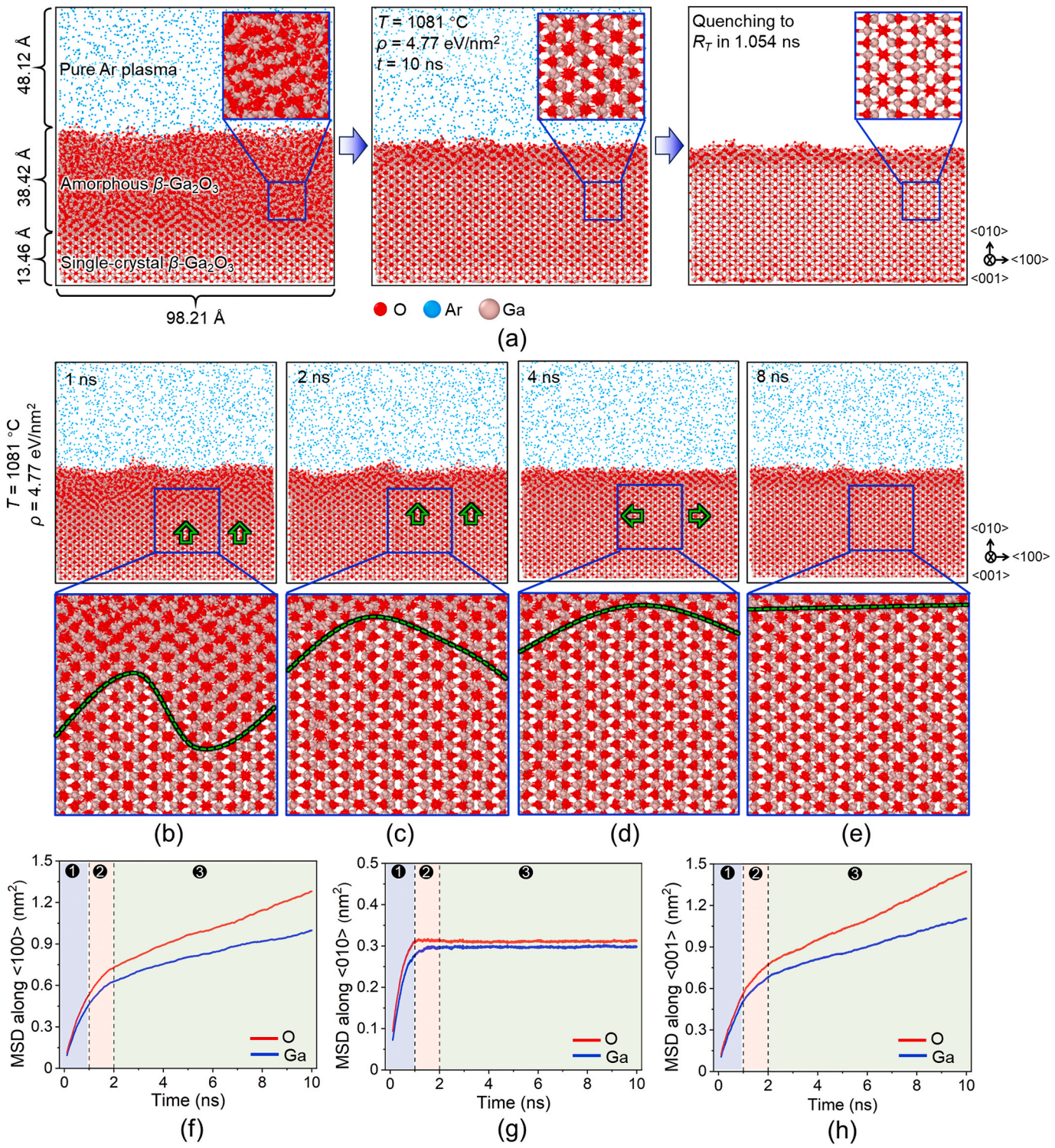

Fig. 17. Large-size molecular dynamics (MD) simulation results at $T = 1081$ °C and $\rho = 4.77$ eV/nm^2. (a) Atomic structures of original model and the final configurations after isothermal and quenching processes, respectively. Structure evolution results at (b) 1, (c) 2, (d) 4, and (e) 8 ns. Mean square displacement (MSD) results along (f) <100>, (g) <010>, and (h) <001> directions.

between HTA and PEAR and reveal the role of the flow field in PEAR of β-Ga_2O_3. The computational details, information on the original models, and detailed discussions are presented in Section 10 of the supplementary information. We find that the thermal field alone cannot induce the significant roughness reduction of β-Ga_2O_3, which is consistent with the results reported in literature [16,37]. However, a combination of the thermal and flow fields can yield a significant reduction in roughness. Fig. 19a,b shows the distributions of the thermal and flow fields at 20 min during the simulation of the step-flow mode, respectively. Under these conditions, the original rough profiles in the left (Fig. 19c) and middle (Fig. 19d) regions of the sample are converted to smooth states. Thus, it is worth emphasizing that the special annealing conditions can distinguish PEAR from conventional HTA methods and that the coupled thermal and flow fields in the plasma should be the impetus for the

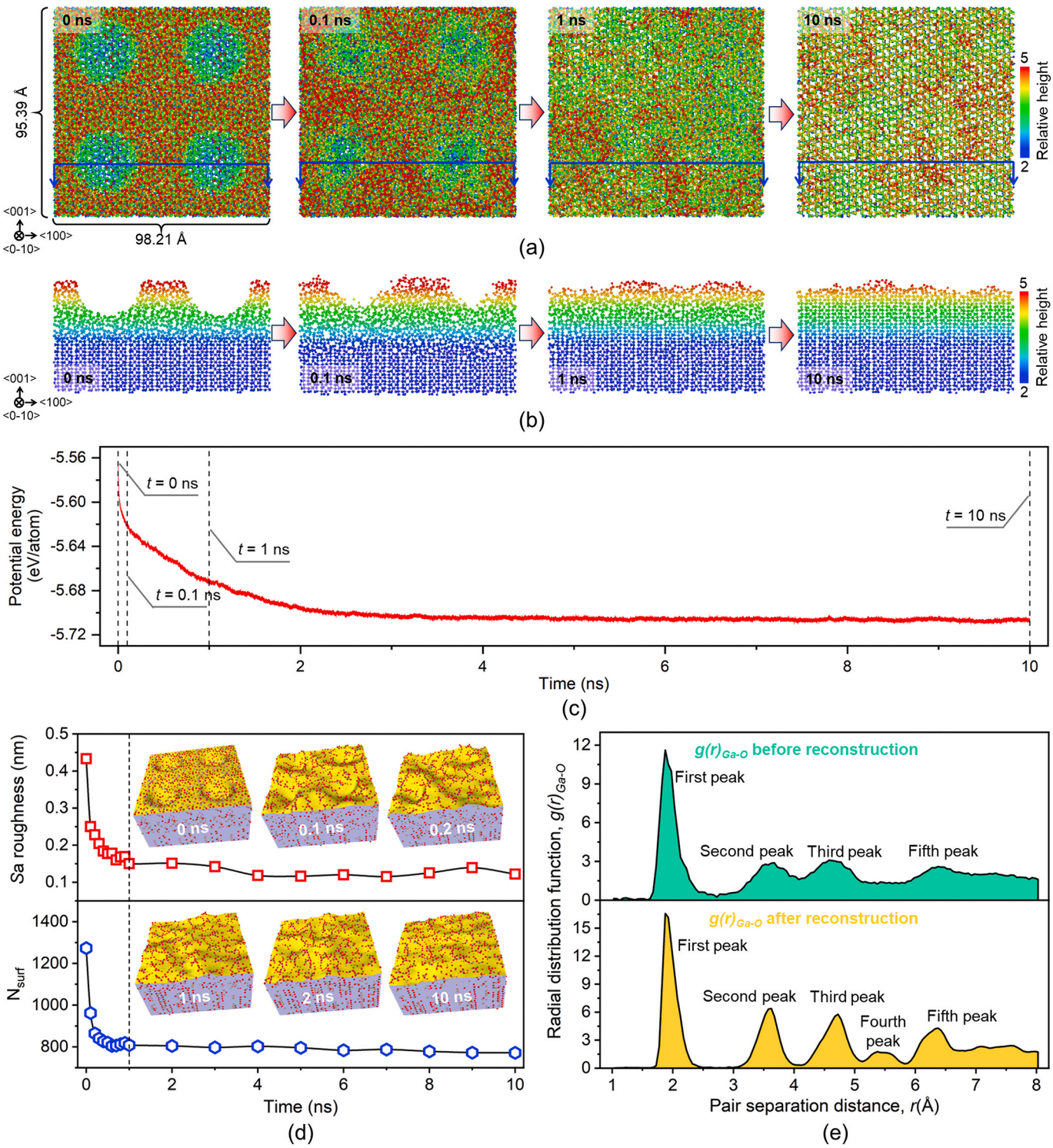

Fig. 18. Roughness and energy analyses for the simulation at $T = 1081$ °C and $\rho = 4.77$ eV/nm^2. (a) Top view and (b) sectional view for height variations of the model during simulation. (c) Potential energy variation. (d) *Sa* roughness and N_{surf} results. The insets are the corresponding surface models at different times. (e) Radial distribution function (RDF) results of Ga–O before and after simulation.

surface reconstruction process.

4.2. *Future development of PEAR and its relationship with ACSM*

Further development of PEAR should involve the processing of large-size TSO wafers. Here, we preliminarily demonstrated PEAR's feasibility in processing a large-size α-Al_2O_3 wafer having the diameter of 25.4 mm, and the results are shown in Fig. 20. Plasma scanning processing (Fig. 20a) can heal all scratches on the as-received α-Al_2O_3 wafer to form relatively uniform step-terrace structures after PEAR (Fig. 20b,c,e), and the significant reductions in *Sa* roughness can be observed (Fig. 20d,f). These results indicate that the PEAR process conducted under atmospheric environment has the potential to achieve atomic-scale smooth surface manufacturing of large-size TSO wafers. However, two issues (cracking and nonuniform reconstruction) still need to be solved, which are thoroughly discussed in Section 11 of the supplementary

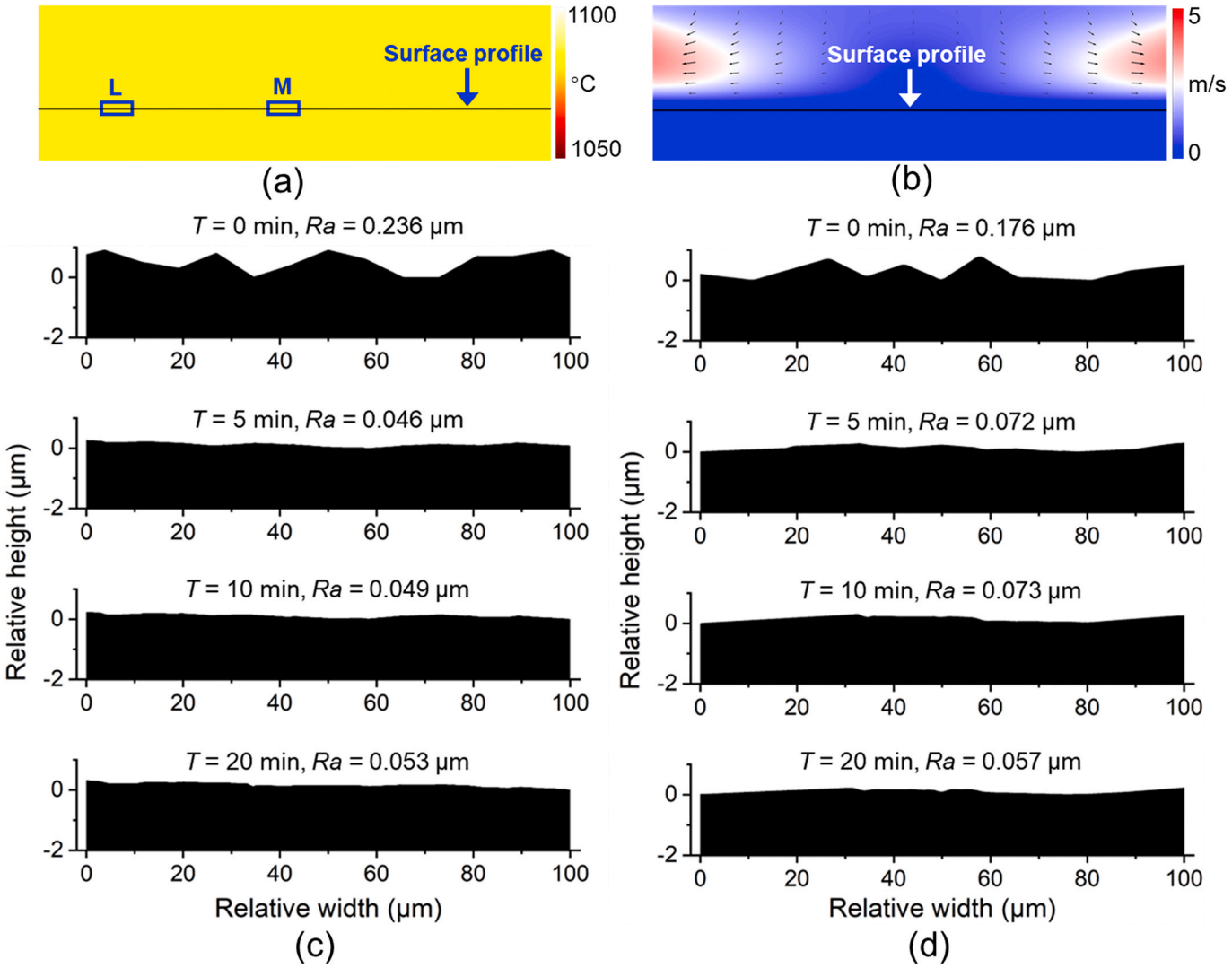

Fig. 19. Numerical simulation results. Distributions of (a) thermal field and (b) flow field in the step-flow mode at 20 min. Surface morphology changes of (c) left (L) and (d) middle (M) regions.

information.

In addition, we summarize the outstanding features of PEAR and discuss the relationship between PEAR and atomic and close-to-atomic scale manufacturing (ACSM) in Section 12 of the supplementary information. First, PEAR is an atomic manufacturing technology without material removal. Second, it can achieve sub-angstrom level roughness. Third, it can result in step-terrace structures. Finally, it shows excellent generality. Hence, PEAR can be regarded as a promising plasma-based ACSM smoothing technology that will enrich the development of ACSM [38,39].

5. Conclusions

Plasma-enabled atomic-scale reconstruction (PEAR) was proposed as a universal atomic-scale smoothing method for wide-bandgap transparent semiconducting oxides (TSOs), including β-Ga_2O_3, α-Al_2O_3, ZnO, and MgO. The surface and subsurface morphological features, surface integrity, and crystalline quality of the PEAR-treated work materials were systematically studied using various characterization techniques. The migration energy barrier of a Ga atom, diffusion and reconstruction behaviors of Ga and O atoms, and role of coupled thermal and flow fields in the plasma were explored by performing multi-scale computations. Furthermore, the feasibility and challenges of the PEAR process for large-size TSO wafers were studied. The following conclusions were drawn.

(1) The input power of the plasma determines the final stable migration mode of the atoms during PEAR. With an increase in the input power, atoms present 2D-island, step-flow, and step-bunching migration modes in sequence. The step-flow migration mode can directly transform a severely damaged β-Ga_2O_3 substrate into a damage-free and atomically smooth surface without any material removal. This process involves the recovery of the subsurface damage layer, the recrystallization of the amorphous layer, and the formation of atomic step-terrace structure. The smooth β-Ga_2O_3 surface shows excellent surface integrity, high crystalline quality, and substantially enhanced photoelectric properties, making β-Ga_2O_3 after PEAR a promising substrate for manufacturing novel electronic devices.

(2) PEAR is a universal approach with high efficiency for atomic surface manufacturing. As exhibited by the (010) surface of β-Ga_2O_3, PEAR can not only achieve the smallest *Sa* roughness (0.098 nm) but also maintain the relatively large roughness reduction rate (24.30 nm/h), when compared with conventional surface finishing techniques such as chemical mechanical polishing (CMP), high temperature annealing (HTA), and wet

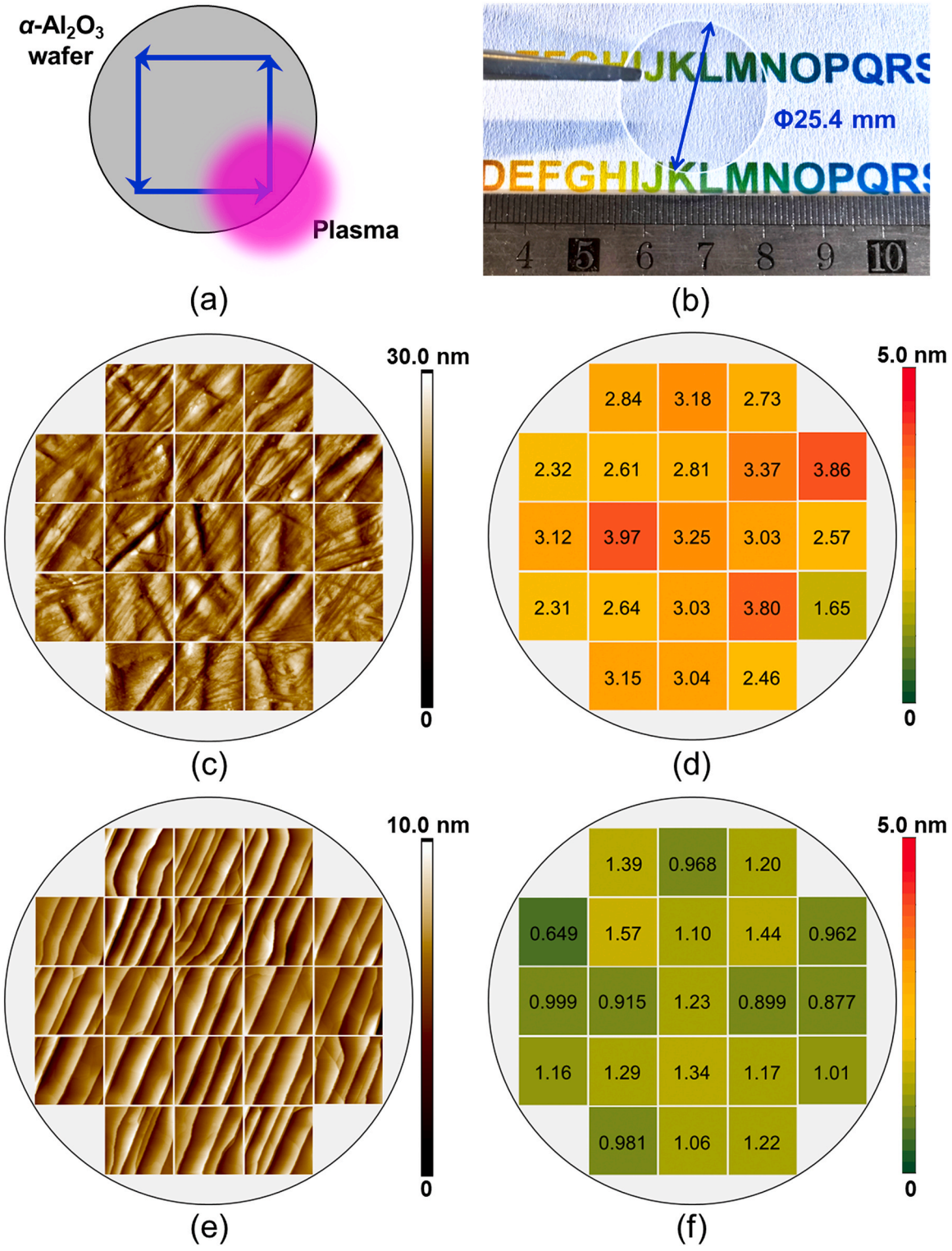

Fig. 20. Plasma-enabled atomic-scale reconstruction (PEAR) results for α-Al_2O_3 (0001) wafer. (a) Schematic diagram for plasma scanning manufacturing. (b) Optical image of α-Al_2O_3 wafer after PEAR. (c) Original surface morphologies of α-Al_2O_3 wafer and (d) corresponding *Sa* roughness distribution obtained by atomic force microscope (AFM). (e) Surface morphologies of α-Al_2O_3 wafer after PEAR and (f) corresponding *Sa* roughness distribution obtained by AFM. All AFM images are recorded in the 1 μm × 1 μm areas.

chemical etching (WCE). Additionally, the smooth α-Al_2O_3, ZnO, and MgO surfaces (*Sa* <0.1 nm) are achieved via PEAR.

(3) The core concept of PEAR is the mass migration and reconstruction of atoms caused by high-energy plasma irradiation. The small migration energy barrier (0.46 eV) calculated at the atomic scale confirms the migration ability of atoms during PEAR. The migration and reconstruction behaviors of atoms at the nanoscale reveal that the O atom always exhibits a larger diffusivity than the Ga atom, and the reconstruction process for the β-Ga_2O_3 (010) substrate first proceeds toward the <010> direction and

then expands along the <100> and <001> directions. The coupling of the thermal and flow fields of the plasma at the millimeter scale serves as the impetus for the migration and reconstruction of atoms.

(4) PEAR can be considered as a novel plasma-based atomic and close-to-atomic scale manufacturing (ACSM) method that may enrich the theoretical and technological knowledge on ACSM. Further work is expected to address the potential cracking and nonuniform reconstruction issues when applying PEAR to large-size TSO wafers.

CRediT authorship contribution statement

Yongjie Zhang: Writing – original draft, Validation, Methodology, Investigation, Formal analysis, Data curation. **Jin Tang:** Visualization, Data curation. **Shaoxiang Liang:** Methodology, Data curation. **Junlei Zhao:** Supervision, Methodology. **Mengyuan Hua:** Methodology. **Chun Zhang:** Supervision, Software, Formal analysis. **Hui Deng:** Writing – review & editing, Supervision, Resources, Project administration, Funding acquisition.

Declaration of competing interest

The authors declare that they have no known competing financial interests or personal relationships that could have appeared to influence the work reported in this paper.

Data availability

Data will be made available on request.

Acknowledgements

This work was supported by the National Natural Science Foundation of China (52375437, 52005243) and the Development and Reform Commission of Shenzhen Municipality (F-2023-Z99-503992). The authors would like to acknowledge the assistance of SUSTech Core Research Facilities.

Appendix A. Supplementary data

Supplementary data to this article can be found online at https://doi.org/10.1016/j.ijmachtools.2024.104119.

References

[1] S.J. Pearton, J. Yang, P.H. Cary, F. Ren, J. Kim, M.J. Tadjer, M.A. Mastro, A review of Ga_2O_3 materials, processing, and devices, Appl. Phys. Rev. 5 (2018) 011301, https://doi.org/10.1063/1.5006941.

[2] J. Zhang, J. Shi, D.-C. Qi, L. Chen, K.H.L. Zhang, Recent progress on the electronic structure, defect, and doping properties of Ga_2O_3, Apl. Mater. 8 (2020) 020906, https://doi.org/10.1063/1.5142999.

[3] Z. Galazka, β-Ga_2O_3 for wide-bandgap electronics and optoelectronics, Semicond. Sci. Technol. 33 (2018) 113001, https://doi.org/10.1088/1361-6641/aadf78.

[4] M. Higashiwaki, K. Sasaki, A. Kuramata, T. Masui, S. Yamakoshi, Gallium oxide (Ga_2O_3) metal-semiconductor field-effect transistors on single-crystal β-Ga_2O_3 (010) substrates, Appl. Phys. Rev. 100 (2012) 013504, https://doi.org/10.1063/1.3674287.

[5] M. Higashiwaki, K. Sasaki, T. Kamimura, M. Hoi Wong, D. Krishnamurthy, A. Kuramata, T. Masui, S. Yamakoshi, Depletion-mode Ga_2O_3 metal-oxide-semiconductor field-effect transistors on β-Ga_2O_3 (010) substrates and temperature dependence of their device characteristics, Appl. Phys. Rev. 103 (2013) 123511, https://doi.org/10.1063/1.4821858.

[6] K. Konishi, K. Goto, H. Murakami, Y. Kumagai, A. Kuramata, S. Yamakoshi, M. Higashiwaki, 1-kV vertical Ga_2O_3 field-plated Schottky barrier diodes, Appl. Phys. Rev. 110 (2017) 103506, https://doi.org/10.1063/1.4977857.

[7] J. Xu, W. Zheng, F. Huang, Gallium oxide solar-blind ultraviolet photodetectors: a review, J. Mater. Chem. C 7 (2019) 8753–8770, https://doi.org/10.1039/c9tc02055a.

[8] C. Huang, H. Zhou, Y. Zhu, C. Xia, Effect of chemical action on the chemical mechanical polishing of β-Ga_2O_3(100) substrate, Precis. Eng. 56 (2019) 184–190, https://doi.org/10.1016/j.precisioneng.2018.11.013.

[9] M.E. Liao, K. Huynh, L. Matto, D.P. Luccioni, M.S. Goorsky, Optimization of chemical mechanical polishing of (010) β-Ga_2O_3, J. Vac. Sci. Technol. 41 (2023) 013205, https://doi.org/10.1116/6.0002241.

[10] C. Huang, W. Mu, H. Zhou, Y. Zhu, X. Xu, Z. Jia, L. Zheng, X. Tao, Effect of OH- on chemical mechanical polishing of β-Ga_2O_3 (100) substrate using an alkaline slurry, RSC Adv. 8 (2018) 6544–6550, https://doi.org/10.1039/c7ra11570a.

[11] Y. Xu, J. Lu, X. Xu, C.-C.A. Chen, Y. Lin, Study on high efficient sapphire wafer processing by coupling SG-mechanical polishing and GLA-CMP, Int. J. Mach. Tool Manufact. 130–131 (2018) 12–19, https://doi.org/10.1016/j.ijmachtools.2018.03.002.

[12] H.-K. Lee, H.-J. Yun, K.-H. Shim, H.-G. Park, T.-H. Jang, S.-N. Lee, C.-J. Choi, Improvement of dry etch-induced surface roughness of single crystalline β-Ga_2O_3 using post-wet chemical treatments, Appl. Surf. Sci. 506 (2020) 144673, https://doi.org/10.1016/j.apsusc.2019.144673.

[13] P. Li, X. Han, D. Chen, Q. Sai, H. Qi, Effect of air annealing on the structural, electrical, and optical properties of V-doped β-Ga_2O_3 single crystals, J. Alloys Compd. 908 (2022) 164590, https://doi.org/10.1016/j.jallcom.2022.164590.

[14] Y. Zhang, A. Mauze, J.S. Speck, Anisotropic etching of β-Ga_2O_3 using hot phosphoric acid, Appl. Phys. Rev. 115 (2019) 013501, https://doi.org/10.1063/1.5093188.

[15] X. Lu, T. Xu, Y. Deng, C. Liao, H. Luo, Y. Pei, Z. Chen, Y. Lv, G. Wang, Performance-enhanced NiO/β-Ga_2O_3 heterojunction diodes fabricated on an etched β-Ga_2O_3 surface, Appl. Surf. Sci. 597 (2022) 153587, https://doi.org/10.1016/j.apsusc.2022.153587.

[16] S. Rafique, L. Han, H. Zhao, Thermal annealing effect on β-Ga_2O_3 thin film solar blind photodetector heteroepitaxially grown on sapphire substrate, Phys. Status Solidi A 214 (2017) 1700063, https://doi.org/10.1002/pssa.201700063.

[17] H. Hu, Z. Feng, Y. Wang, Y. Liu, H. Dong, Y.-Y. Liu, Y. Hao, G. Han, The role of surface pretreatment by low temperature O_2 gas annealing for β-Ga_2O_3 Schottky barrier diodes, Appl. Phys. Rev. 120 (2022) 073501, https://doi.org/10.1063/5.0080343.

[18] Z. Fang, Y. Zhang, R. Li, Y. Liang, H. Deng, An efficient approach for atomic-scale polishing of single-crystal silicon via plasma-based atom-selective etching, Int. J. Mach. Tool Manufact. 159 (2020) 103649, https://doi.org/10.1016/j.ijmachtools.2020.103649.

[19] H. Deng, Y. Zhang, J. Liang, X. Zhang, Surface reconstruction of sapphire at the atomic scale via chemical-physical tuning of atmospheric plasma, CIRP Ann. Manuf. Technol. 72 (2023) 489–492, https://doi.org/10.1016/j.cirp.2023.04.011.

[20] H. Nakahara, M. Ichikawa, Migration of Ga atoms during Si molecular beam epitaxial growth on a Ga-adsorbed Si(111) surface, Surf. Sci. 298 (1993) 440–449, https://doi.org/10.1016/0039-6028(93)90059-S.

[21] S. Bin Anooz, R. Grüneberg, C. Wouters, R. Schewski, M. Albrecht, A. Fiedler, K. Irmscher, Z. Galazka, W. Miller, G. Wagner, J. Schwarzkopf, A. Popp, Step flow growth of β-Ga_2O_3 thin films on vicinal (100) β-Ga_2O_3 substrates grown by MOVPE, Appl. Phys. Rev. 116 (2020) 182106, https://doi.org/10.1063/5.0005403.

[22] R.F. Xiao, N.B. Ming, Surface roughening and surface diffusion in kinetic thin-film deposition, Phys. Rev. E 49 (1994) 4720–4723, https://doi.org/10.1103/physreve.49.4720.

[23] S. Vézian, F. Natali, F. Semond, J. Massies, From spiral growth to kinetic roughening in molecular-beam epitaxy of GaN(0001), Phys. Rev. B 69 (2004) 125329, https://doi.org/10.1103/PhysRevB.69.125329.

[24] S.T. Pantelides, Temperature effects in atomic diffusion in silicon, Phys. Rev. B 36 (1987) 3462–3464, https://doi.org/10.1103/physrevb.36.3462.

[25] K. Bellmann, U.W. Pohl, C. Kuhn, T. Wernicke, M. Kneissl, Controlling the morphology transition between step-flow growth and step-bunching growth, J. Cryst. Growth 478 (2017) 187–192, https://doi.org/10.1016/j.jcrysgro.2017.09.007.

[26] Y. Yao, Y. Ishikawa, Y. Sugawara, X-ray diffraction and Raman characterization of β-Ga_2O_3 single crystal grown by edge-defined film-fed growth method, J. Appl. Phys. 126 (2019) 205106, https://doi.org/10.1063/1.5129226.

[27] K. Zhang, Z. Xu, S. Zhang, H. Wang, H. Cheng, J. Hao, J. Wu, F. Fang, Raman and photoluminescence properties of un-/ion-doped β-Ga_2O_3 single-crystals prepared by edge-defined film-fed growth method, Phys. Rev. B 600 (2021) 412624, https://doi.org/10.1016/j.physb.2020.412624.

[28] C. Liu, Y. Berencén, J. Yang, Y. Wei, M. Wang, Y. Yuan, C. Xu, Y. Xie, X. Li, S. Zhou, Irradiation effects on the structural and optical properties of single crystal β-Ga_2O_3, Semicond. Sci. Technol. 33 (2018) 095022, https://doi.org/10.1088/1361-6641/aad8d1.

[29] X. Chen, Y. Gu, J. Lin, A. Yi, M. Kang, X. Cang, Study on subsurface damage and surface quality of silicon carbide ceramic induced by a novel non-resonant vibration-assisted roll-type polishing, J. Mater. Process. Technol. 282 (2020) 116667, https://doi.org/10.1016/j.jmatprotec.2020.116667.

[30] S. Li, Z. Wang, Y. Wu, Relationship between subsurface damage and surface roughness of optical materials in grinding and lapping processes, J. Mater. Process. Technol. 205 (2008) 34–41, https://doi.org/10.1016/j.jmatprotec.2007.11.118.

[31] T. Sugihara, R. Kobayashi, T. Enomoto, Direct observations of tribological behavior in cutting with textured cutting tools, Int. J. Mach. Tool Manufact. 168 (2021) 103726, https://doi.org/10.1016/j.ijmachtools.2021.103726.

[32] C. Tan, R. Li, J. Su, D. Du, Y. Du, B. Attard, Y. Chew, H. Zhang, E.J. Lavernia, Y. Fautrelle, J. Teng, A. Dong, Review on field assisted metal additive manufacturing, Int. J. Mach. Tool Manufact. 189 (2023) 104032, https://doi.org/10.1016/j.ijmachtools.2023.104032.

[33] J. Zhao, J. Byggmästar, H. He, K. Nordlund, F. Djurabekova, M. Hua, Complex Ga_2O_3 polymorphs explored by accurate and general-purpose machine-learning

interatomic potentials, npj Comput. Mater. 9 (2023) 159, https://doi.org/10.1038/s41524-023-01117-1.
[34] M.F. Lovisa, G. Ehrlich, Quantitative determinations of the temperature dependence of diffusion phenomena in the FIM, Surf. Sci. 246 (1991) 43–49, https://doi.org/10.1016/0039-6028(91)90390-E.
[35] J.H. Neave, P.J. Dobson, B.A. Joyce, J. Zhang, Reflection high-energy electron diffraction oscillations from vicinal surfaces—a new approach to surface diffusion measurements, Appl. Phys. Rev. 47 (1985) 100–102, https://doi.org/10.1063/1.96281.
[36] S. Banerjee, X. Jiang, L.W. Wang, Designing a porous-crystalline structure of β-Ga_2O_3: a potential approach to tune its opto-electronic properties, Phys. Chem. Chem. Phys. 20 (2018) 9471–9479, https://doi.org/10.1039/C7CP08565F.
[37] B. Feng, G. He, X. Zhang, X. Chen, Z. Li, L. Xu, R. Huang, J. Feng, Y. Wu, Z. Jia, H. Yu, Z. Zeng, S. Ding, The effect of annealing on the Sn-doped (−201) β-Ga_2O_3 bulk, Mater. Sci. Semicond. Process. 147 (2022) 106752, https://doi.org/10.1016/j.mssp.2022.106752.
[38] J. Gao, X. Luo, F. Fang, J. Sun, Fundamentals of atomic and close-to-atomic scale manufacturing: a review, Int. J. Extrem. Manuf. 4 (2021) 012001, https://doi.org/10.1088/2631-7990/ac3bb2.
[39] F. Fang, On the three paradigms of manufacturing advancement, Nanomanuf. Metrol. 6 (2023) 1–3, https://doi.org/10.1007/s41871-023-00217-2.